MICROCOPY RESOLUTION TEST CHART

NATIONAL BUREAU OF STANDARDS-1963-A
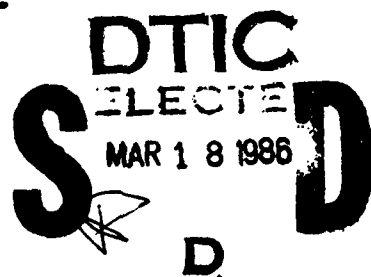
⑫

RADC-TR-85-160
Interim Report
January 1986

A HYBRID-ITERATIVE TECHNIQUE FOR COMPLEX SCATTERING PROBLEMS

AD-A165 233

University of Dayton

P. Krishna Murthy
Kuei-Chien C. Shill
Gary A. Thiele

DTIC
ELECTE
MAR 1 8 1986
S
D

DTIC FILE COPY

ROME AIR DEVELOPMENT CENTER
Air Force Systems Command
Griffiss Air Force Base, NY 13441-5700

AD-A165 233

REPORT DOCUMENTATION PAGE

1a. REPORT SECURITY CLASSIFICATION UNCLASSIFIED		1b. RESTRICTIVE MARKINGS N/A		
2a. SECURITY CLASSIFICATION AUTHORITY N/A		3. DISTRIBUTION/AVAILABILITY OF REPORT Approved for public release; distribution unlimited.		
2b. DECLASSIFICATION/DOWNGRADING SCHEDULE N/A				
4. PERFORMING ORGANIZATION REPORT NUMBER(S) UDR-TR-85-56		5. MONITORING ORGANIZATION REPORT NUMBER(S) RADC-TR-85-160		
6a. NAME OF PERFORMING ORGANIZATION University of Dayton	6b. OFFICE SYMBOL (If applicable)	7a. NAME OF MONITORING ORGANIZATION Rome Air Development Center (EECT)		
6c. ADDRESS (City, State, and ZIP Code) Graduate Engineering & Research School of Engr 300 College Park Dayton OH 45469		7b. ADDRESS (City, State, and ZIP Code) Hanscom AFB MA 01731		
8a. NAME OF FUNDING/SPONSORING ORGANIZATION Rome Air Development Center	8b. OFFICE SYMBOL (If applicable) EECT	9. PROCUREMENT INSTRUMENT IDENTIFICATION NUMBER F19628-83-K-0034		
8c. ADDRESS (City, State, and ZIP Code) Hanscom AFB MA 01731		10. SOURCE OF FUNDING NUMBERS		

	PROGRAM ELEMENT NO 62702F	PROJECT NO 4600	TASK NO 15	WORK UNIT ACCESSION NO 68

11. TITLE (Include Security Classification)

A HYBRID-ITERATIVE TECHNIQUE FOR COMPLEX SCATTERING PROBLEMS

12. PERSONAL AUTHOR(S)
P. Krishna Murthy, Kuei-Chien C. Shill, Gary A. Thiele

13a. TYPE OF REPORT Interim	13b. TIME COVERED FROM May 84 TO May 85	14. DATE OF REPORT (Year, Month, Day) January 1986	15. PAGE COUNT 64

16. SUPPLEMENTARY NOTATION

N/A

17. COSATI CODES			18. SUBJECT TERMS (Continue on reverse if necessary and identify by block number)
FIELD	GROUP	SUB-GROUP	Iterative Diffraction
12	01		Bistatic Scattering Hybrid
20	14		

19. ABSTRACT (Continue on reverse if necessary and identify by block number)

A new technique, named a hybrid-iterative technique, is presented which computes the induced currents on an arbitrary, perfectly conducting scatterer. The technique is an evolution from two previous techniques developed earlier. The first of the previous techniques used the moment method to compute correction currents to an optics-type current. The second of the previous techniques, which was developed on this contract, effected a significant improvement by eliminating the use of the moment method to obtain the correction currents, using iteration to obtain them. The technique described here incorporates the edge diffraction theory and the Fock theory into the ansatz of the iterative scheme. This procedure speeds up the algorithm as well as extending the range of problems that can be solved by the iterative scheme. Furthermore, the technique described in this report incorporates the correction currents into the optics currents thereby substantially reducing the computation time. For intermediate size and larger bodies, the CPU time is significantly less than that of the moment method. Results are presented for a variety of curved and edged two-dimensional cylinders.

20. DISTRIBUTION/AVAILABILITY OF ABSTRACT ☐ UNCLASSIFIED/UNLIMITED ☒ SAME AS RPT ☐ DTIC USERS	21. ABSTRACT SECURITY CLASSIFICATION UNCLASSIFIED	
22a. NAME OF RESPONSIBLE INDIVIDUAL Robert V. McGahan	22b. TELEPHONE (Include Area Code) (513) 229-2241	22c. OFFICE SYMBOL RADC (EECT)

TABLE OF CONTENTS

LIST OF FIGURES

I. INTRODUCTION

Kim and Thiele [1] have developed a hybrid AS-MM technique (asymptotic-moment method technique) to find the induced currents on the surface of scatterers in the intermediate frequency region. Kaye, Murthy and Thiele [2], [3] have significantly improved on that work by eliminating the moment method regions thereby making the method potentially applicable to large scatterers as well as ones of modest size. In the work of Kaye, Murthy and Thiele, the MFIE was reduced to a sequence of integral equations for both the "optics" currents and the "correction" currents, each of which is solved by iteration. On the other hand, in Kim and Thiele [1], the "correction" currents were solved by the moment method. The present technique, then, is a purely iterative technique wherein all the integral equations are of the same form and are similarly solved via iteration. In this report, the iterative method is improved still further by reducing the amount of computation required as discussed below.

In this report we present further investigations on the iterative technique [2]. In [3], the optics currents on the lit side are computed assuming that the shadow-side current is zero. Hence, any two scatterers whose lit-side geometry is the same would have identical "optics" currents on the lit-side, notwithstanding the fact that the shadow-side geometry is different. The effect of the shadow-side geometry is taken into account while computing the correction currents on the lit side. This necessitates the computation of higher-order correction currents. Furthermore, there are situations when the approximation of the shadow-side current by zero current is inappropriate. As an example, consider the situation of a square cylinder

1

being illuminated by a plane wave when the angle of incidence is such that one of the faces in the shaow region is near grazing. The current on that face is quite appreciable and cannot be taken to be zero. We, therefore, modify the iterative technique by incorporating the effect of shadow-side currents for a scatterer with either surface discontinuities or a smooth surface. To obtain these initial currents, we developed closed form expressions for currents on a wedge. For smooth bodies, Fock theory [4] furnishes the initial estimates of the shadow-side current. Thus, we incorporate the edge diffraction theory and Fock theory into the ansatz for the iterative technique and obtain the hybrid-iterative technique. We are also able to recast the integral equations for correction currents in such a way that the technique consists in computing the optics currents over and again. This effects a considerable simplification of the computer program. Furthermore, incorporating the initial currents into the iterative technique removed the necessity of computing the higher order correction currents. Indeed, frequently the zeroth-order optics currents themselves are a sufficiently accurate solution.

In Section II, we develop the integral equations and discuss their solution by iteration. In Section III, we present theory relevant to the initial estimates of the shadow-side currents for both smooth bodies and edged bodies. In Section IV, we deal with some special numerical considerations. Section V presents extensive computations illustrating the theory developed in Section II. Both edged bodies, exemplified by a square cylinder and smooth bodies exemplified by circular and elliptic cylinders are considered. Section V contains summary of the technique and points out further avenues of research.

II. GENERAL THEORY

A. MAGNETIC FIELD INTEGRAL EQUATION

Consider a perfectly conducting body illuminated by a plane wave. The induced surface current density on the body at an observation point P (see Fig. 1) can be computed from the MFIE:

$$\vec{J}(\vec{R}) = 2\hat{n} \times \vec{H}_i(\vec{R}) + 2\hat{n} \times L[\vec{J}] \tag{1}$$

where the operator L is defined by

$$L[\vec{J}] = \int_{\Sigma} \vec{J}(\vec{R}') \times \vec{\nabla}'G(r) \, ds' \quad . \tag{2}$$

The surface of the body is denoted by Σ and $\vec{R}$ and $\vec{R}'$ are the observation and source point position vectors, respectively, on Σ and $r = |\vec{R} - \vec{R}'|$. The prime on the gradient operator indicates that the differentiation is performed on the source coordinates. The bar through the integral sign is used to denote the principle value integral over Σ. $\vec{H}^i$ is the incident magnetic field vector and $\hat{n}$ is the outward unit normal to the surface at $\vec{R}$. $G(r)$ is the free-space Green's function given by

$$G(r) = \frac{e^{-j\beta r}}{4\pi r} \tag{3}$$

for the three-dimensional problem and by

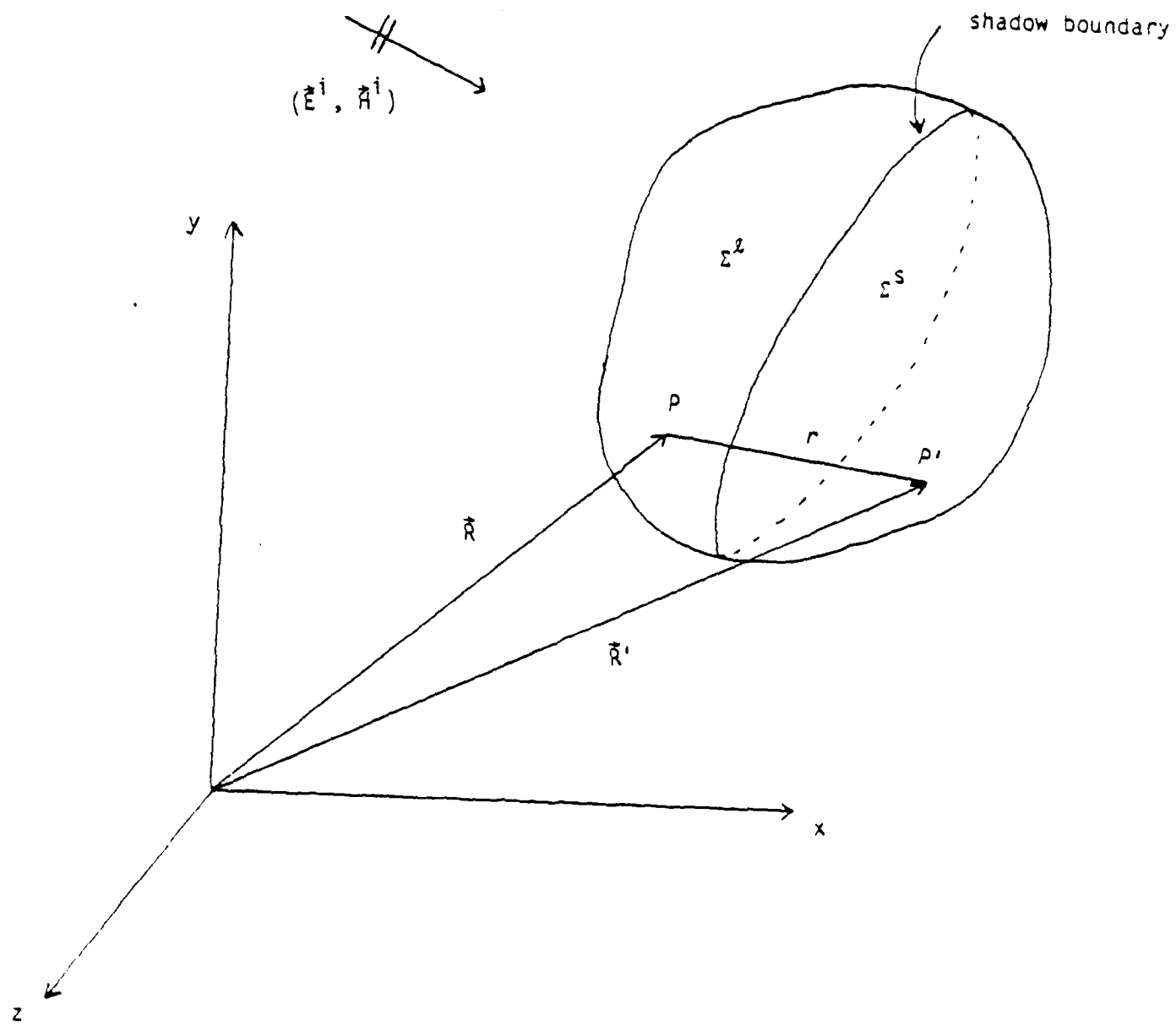$$G(r) = \frac{1}{4j} H_o^{(2)}(\beta r) \tag{4}$$

Figure 1. Scattering by a perfectly conducting body.

4

for the two-dimensional problem. $H_0^{(2)}(\beta r)$ is the zero-order Hankel function of the second kind and β is the free space propagation constant. The time dependence is taken to be $\exp(j\omega t)$ and is suppressed throughout.

B. OPTICS CURRENTS

The first step in solving the MFIE for the induced surface current density $\vec{J}(\vec{R})$ is to divide the total surface Σ of the body into Σ^ℓ and Σ^S, which represents the lit and shadowed regions, respectively. The dividing line between these two regions is the geometrical optics shadow boundary which is defined as the locus of points satisfying $\hat{u} \cdot \hat{n} = 0$, where $\hat{u}$ is the unit vector in the direction of propagation of the incident field. Then $\vec{J}(\vec{R})$ can be expressed as follows:

$$\vec{J}(\vec{R}) = \delta\vec{J}^\ell(\vec{R}) + (1 - \delta)\vec{J}^S(\vec{R}) \tag{5}$$

where $\delta = 1$ if $\vec{R} \in \Sigma^\ell$ and $\delta = 0$ if $\vec{R} \in \Sigma^S$. Eq. (1) can now be rewritten as:

$$\vec{J}(\vec{R}) = 2\hat{n}x \, \vec{H}_i(\vec{R}) + 2\hat{n}x \, L[\vec{J}^\ell] + 2\hat{n}x \, L[\vec{J}^S] . \tag{6}$$

In the notation used in Eq. (6) and in subsequent equations, the surface of integration is identified by the superscript on the current density. We now write out Eq. (6) explicitly for $\vec{R} \in \Sigma^\ell$ and $\vec{R} \in \Sigma^S$:

$$\vec{J}^\ell(\vec{R}) = 2\hat{n}x \, \vec{H}_i(\vec{R}) + 2\hat{n}x \, L[\vec{J}^\ell] + 2\hat{n}x \, L[\vec{J}^S] \tag{7}$$

$$\vec{J}^S(\vec{R}) = 2\hat{n}x \, \vec{H}_i(\vec{R}) + 2\hat{n}x \, L[\vec{J}^\ell] + 2\hat{n}x \, L[\vec{J}^S] \tag{8}$$

5

The problem of solving for the induced surface current density has now been transformed into one of solving Eqs. (7) and (8) for J^ℓ and J^S. We compute these currents in sequential fashion in the following way.

First, let J_E^S be an estimate of shadow current. For edged bodies like the square cylinder, this current is obtained from the wedge diffraction theory. For smooth bodies like circular or elliptic cylinders, this current is obtained using Fock theory. A detailed discussion of determining J_E^S will be considered in Section III. Thus,

$$. \quad J^S \sim J_E^S \tag{9}$$

Substituting Eq. (9) in Eq. (7) and noting that the current on the lit side would now be an approximation to the true current and denoting this approximate current by J_{op}^ℓ,

$$J_{op}^\ell = 2\hat{n}x\ H_i(\vec{R}) + 2\hat{n}x\ L[J_{op}^\ell] + 2\hat{n}x\ L[J_E^S] \tag{10}$$

This "optics current" is a significant improvement over the classical physical optics (PO) current since it takes into account mutual interaction of current on both lit- and shadow-regions in addition to the geometrical optics (GO) field.

A shadow-side "optics current", J_{op}^S, is now defined by substituting $J^\ell = J_{op}^\ell$ in (8):

$$J_{op}^S(\vec{R}) = 2\hat{n}x\ H_i(\vec{R}) - 2\hat{n}x\ L[J_{op}^\ell] + 2\hat{n}x\ L[J_{op}^S] \tag{11}$$

6

In this expression, the main contribution of the second term on the right-hand side will be $-2\hat{n}x\, \vec{H}_i(\vec{R})$ to cancel the first term. The $\vec{J}_{op}^{S}$ obtained from Eq. (11) would be closer to the true current than our initial guess $\vec{J}_E^S$. Indeed, the only inaccuracy incurred being that through the approximate value taken for the lit-side current.

Now that a better approximation to the shadow-side current is available than is $\vec{J}_E^S$, a new optics current on the lit side may be obtained. This lit-side current may be used to further improve the shadow-side current. Thus, higher-order optics currents may be obtained until the desired accuracy is achieved. The integral equations for nth order optics currents may be defined as follows

$$\vec{J}_{op,n}^{\ell} = 2\hat{n}x\, \vec{H}_i(\vec{R}) + L[\vec{J}_{op,n}^{\ell}] + L[\vec{J}_{op,n-1}^{S}] \tag{12}$$

$$\vec{J}_{op,n}^{S} = 2\hat{n}x\, \vec{H}_i(\vec{R}) + L[\vec{J}_{op,n}^{\ell}] + L[\vec{J}_{op,n}^{S}] \tag{13}$$

$$n = 1, 2 \ldots$$

$\vec{J}_{op,o}^{S}$ is the solution of Eq. (11).

In the iterative technique described in an earlier report, the optics current of zeroth order were improved upon by the addition of correction currents. The technique described here is mathematically equivalent to the correction current ansatz of the iterative technique and at the same time is much simpler from the programming point of view.

7

Thus, the hybrid-iterative technique computes the currents on the lit and shadow regions in sequential fashion starting with an initial estimate for the shadow current. All the integral equations are of the same form and are, in fact, Fredholm integral equations of the second kind. Hence, all these integrals may be solved by iteration as discussed in [2], [3].

III. INITIAL CURRENTS

An initial estimate of the current on a scatterer with surface discontinuities like a square cylinder is obtained from a knowledge of currents on a wedge. For a scatterer with smooth surface, Fock theory may be used to obtain the initial estimate of the shadow-side current.

A. Shadow-Side Current on a Wedge:

Consider the wedge shown in Figure 2 illuminated by a TE-plane wave. When the angle of incidence ϕ_i is such that the shadow boundary is not "close" to face B, the current on face B is given by [5],

$$J_E^S = -4 \frac{H_o}{n} K_- (x_B) e^{-i\beta\rho} \hat{t}_B \quad \begin{array}{l} 0 \le \rho \le \infty \\ 0 \le \phi_i \le (n-1)\pi - \frac{n\pi}{10} \end{array} \tag{14}$$

where,

$$K_- (x) = \sqrt{\frac{i}{\pi}} e^{ix^2} \int_X^\infty e^{-it^2} dt \quad .$$

$$x_B = \sqrt{2\beta\rho_B} \cdot (\cos \frac{\pi}{n} + \cos \frac{\phi_i}{n})/\sin \frac{\pi}{n}$$

β = propagation constant

ρ = distance from the edge

$n = (2 - \frac{\alpha}{\pi})$

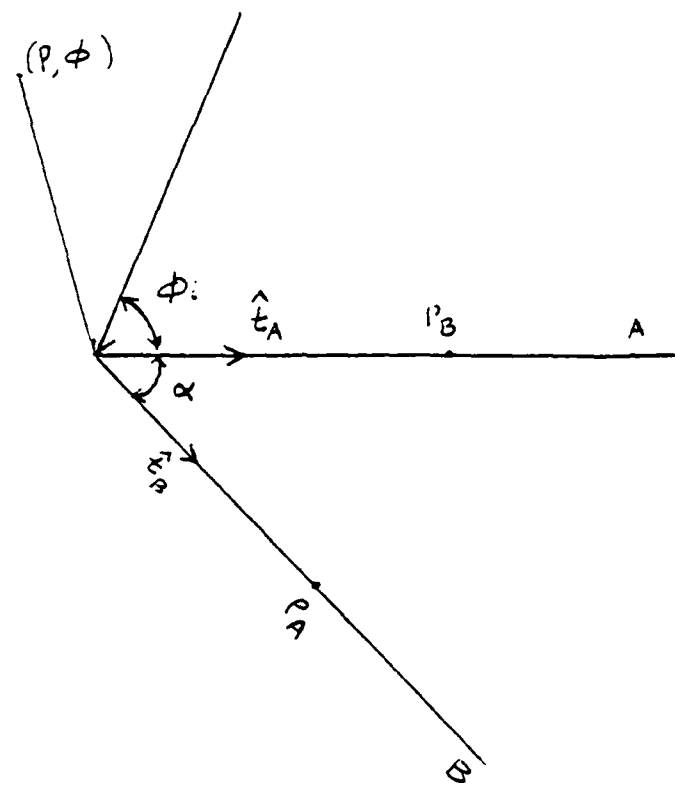α = interior wedge angle.

9

Figure 2. Geometry of a wedge.

When the angle of incidence is such that a shadow boundary is close to face B, the current is given by,

$$\vec{J}_E^S = -2H_0[B \ K_-\ (Bx_B^-) + \text{sgn}(\cot\psi^+) \ K_-\ (x_B^+)] \ e^{-j\beta\rho} \ \hat{t}_B$$

$$0 < \rho < \infty$$

$$(n-1)\pi - \frac{n\pi}{10} < \phi_i < (n-1)\pi \ . \tag{15}$$

where, $B = (\frac{2}{n} - 1)$

$$x_B^\pm = \sqrt{\beta\rho/2} \cdot 2n \cot \psi^\pm$$

$$\psi^\pm = (\pi \pm \phi_i)/2n$$

Thus, Equations (14) and (15) express the currents on the shadow side of a wedge in closed form. These expressions involve the well-known modified Fresnel functions, $K_-\ (x)$ [6] and are easy to compute. Figure 3 presents shadow-side currents on wedge computed using the above expressions as well as the exact solution obtained from the eigenfunction solution. Note that the agreement is excellent.

These currents on the wedge may readily be used to obtain an initial estimate of the shadow current on a square cylinder. Consider the geometry of a square cylinder shown in Figure 4. Faces 2 and 3 are in the shadow region. Faces 1 and 2 constitute a wedge illuminated with the angle of

11
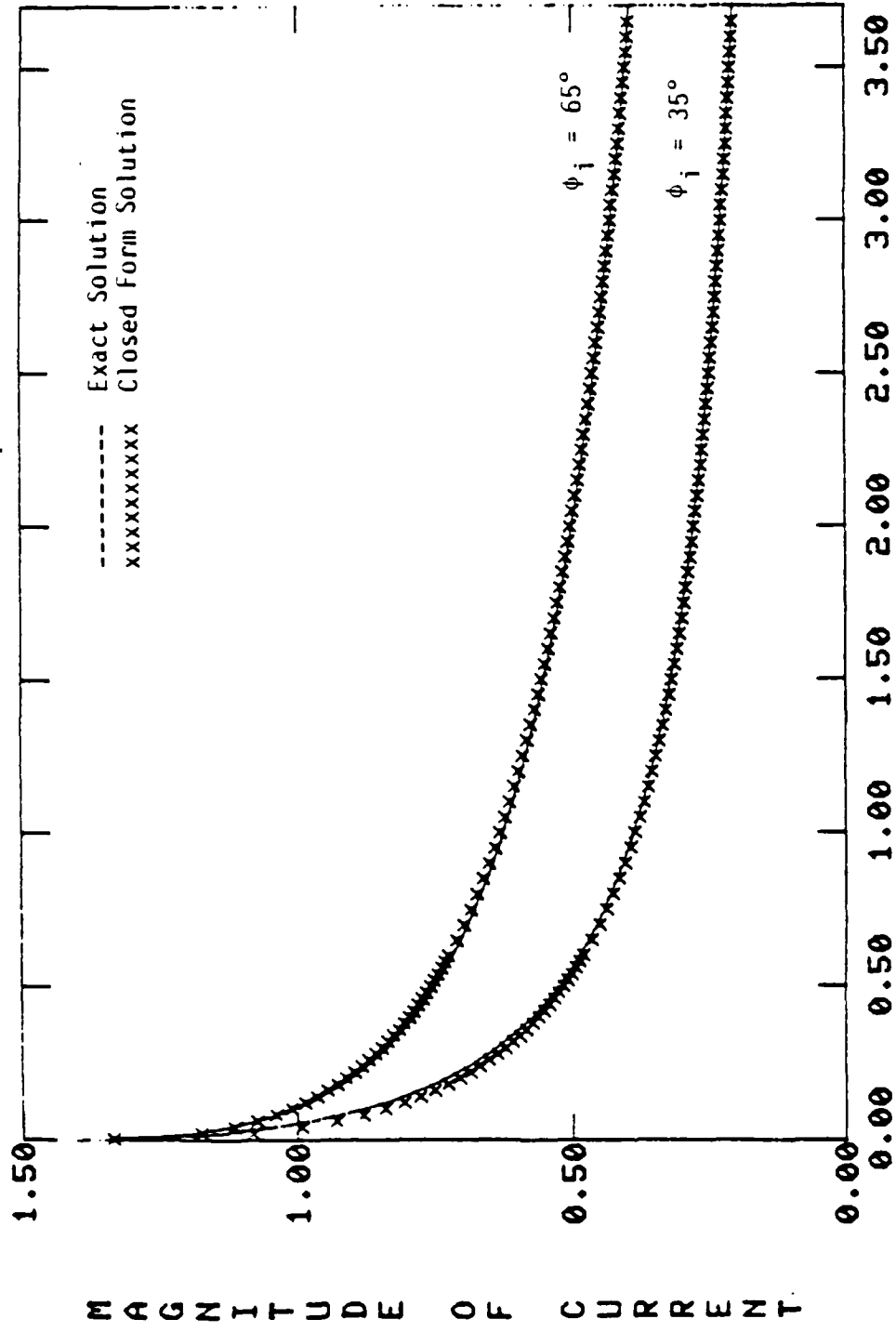
DISTANCE FROM EDGE (WAVELENGTHS)

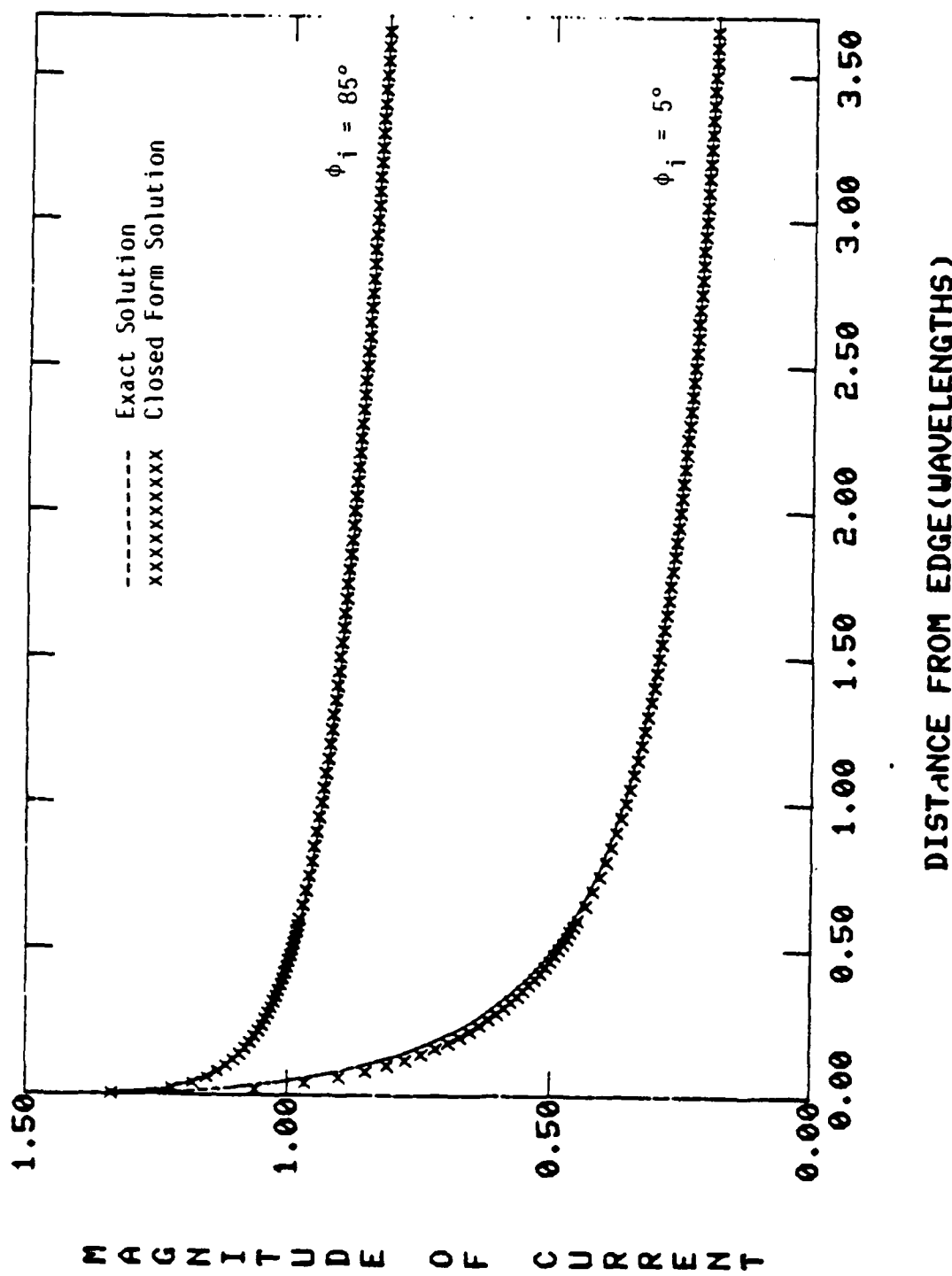Figure 3a. Shadow-side currents on wedge.

$\alpha = 90^{\circ}$

12

DISTANCE FROM EDGE(WAVELENGTHS)

Figure 3b. Shadow-side currents on wedge.
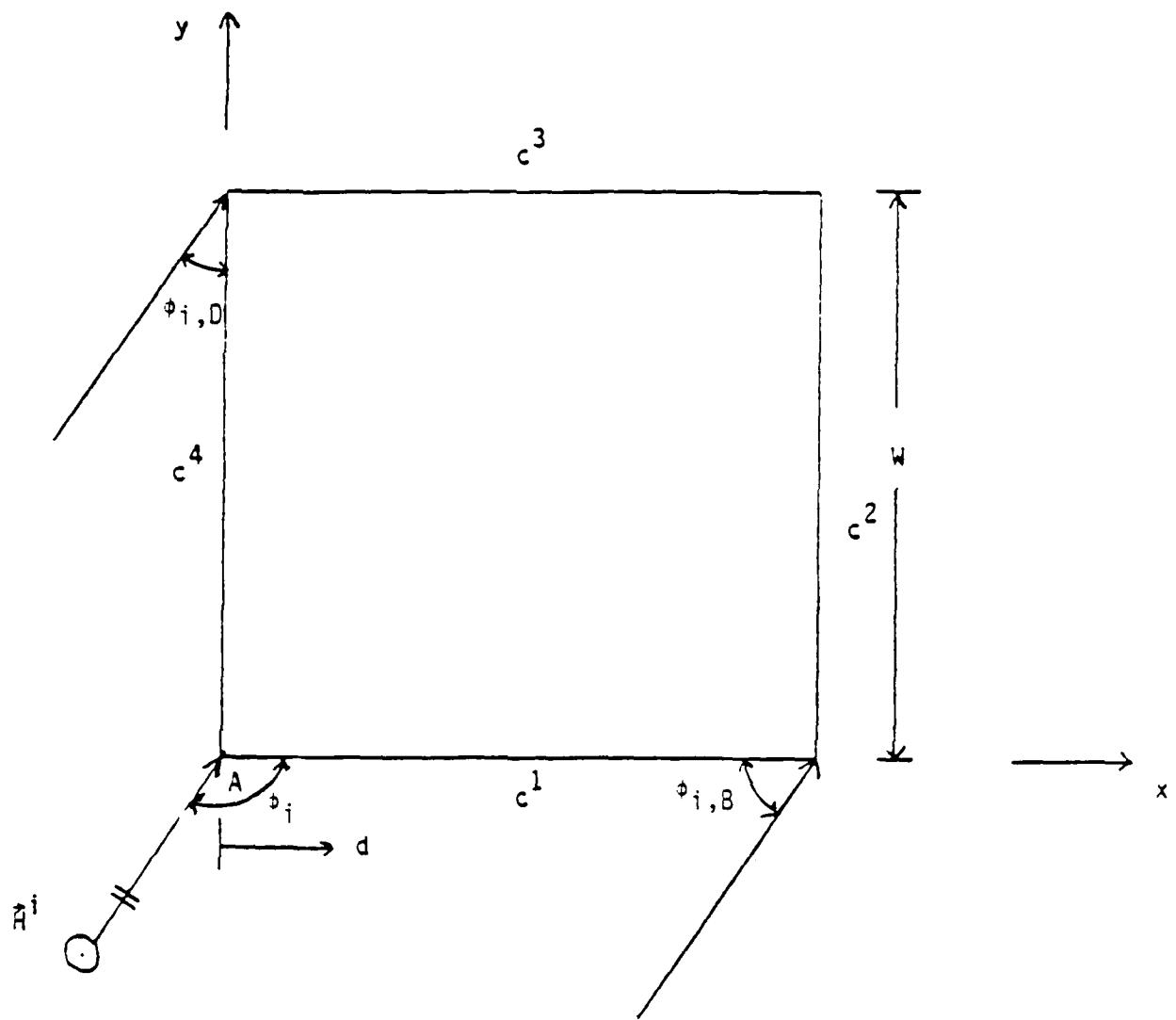
$\alpha = 90°$

13

Figure 4. Geometry for square cylinder.

incidence being $\phi_{i,B}$. The current on face 2 may be approximated by the current on a corresponding wedge with $\alpha = \pi/2$ and $\phi_i = \phi_{i,B}$. In a similar fashion, the current on face 3 also may be approximated.

B. Shadow-Side Current on a Smooth Body:

From Fock's theory [4], the tangential components H_{tg} of the magnetic field on the surface of a smooth perfectly conducting body are equal to the tangential components of the external field H_{tg}^{ex} multiplied by a universal function of the reduced distance ξ. Therefore, for TE polarization

$$H_{tg} = H_{tg}^{ex} \; g(\xi) \tag{16}$$

where

$$g(\xi) = e^{-j\frac{\xi^3}{3}} \; \frac{1}{\sqrt{\pi}} \int_C e^{-j\xi t} \; \frac{dt}{W_1(t)} \tag{17}$$

The expression for the Airy function W_1 and the contour C are given in [4]. For the definition of ξ and H_{tg}^{ex}, let us consider the case where the perfectly conducting body is an infinite circular cylinder of radius 'a' with its axis oriented in the z direction and a plane wave is incident along the negative y axis with the magnetic field also in the z direction, as shown in Figure 5. According to Goodrich [7], the distance from the shadow boundary originally given in Fock's theory has been generalized to the arc length on the surface of the cylinder from the shadow boundary. Therefore, the magnetic field on the cylinder surface H_z is given by

$$H_z = H_0 \sum_{n=0}^{\infty} \left\{ e^{-j\beta \ell_{1n}} g(\xi_{1n}) + e^{-j\beta \ell_{2n}} g(\xi_{2n}) \right\} \tag{18}$$
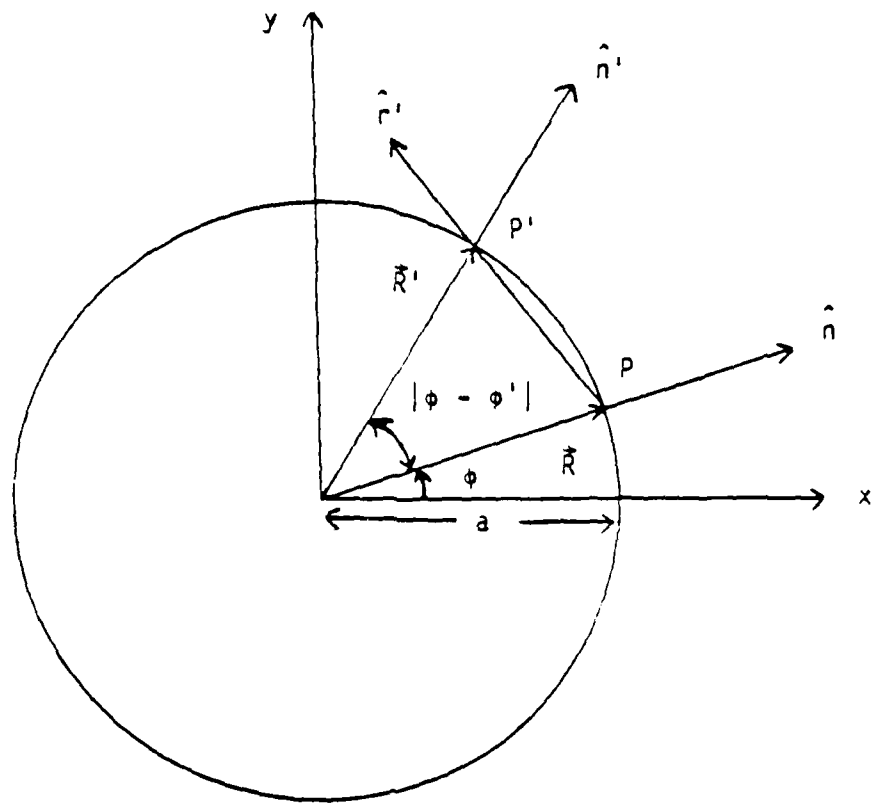
Figure 5. Geometry for circular cylinder.

where H_0 is the magnitude of the incident plane wave and $g(\xi)$ is defined the same way as above. β is the propagation constant and ℓ_{1n} and ℓ_{2n} are the arc lengths on the cylinder surface given by

$$\ell_{1n} = a(\phi_1 + 2n\pi)$$
$$\ell_{2n} = a(\phi_2 + 2n\pi) \tag{19}$$

where

$$\phi_1 = 2\pi - \phi, \text{ and}$$
$$\phi_2 = \phi - \pi \tag{20}$$

as shown in Figure 5 with $0 < \phi < 2\pi$. The reduced distances corresponding to these path lengths are given by

$$\xi_{1n} = (\frac{\beta a}{2})^{1/3} (\phi_1 + 2n\pi)$$
$$\xi_{2n} = (\frac{\beta a}{2})^{1/3} (\phi_2 + 2n\pi) \; . \tag{21}$$

Since $g(\xi)$ decreases monotonically away from the shadow boundary, after the wave creeps along the cylinder surface more than half of the circle, the field decays to an insignificant value. Therefore, only the first term of the series is retained.

Once the field on the surface is found, one can obtain the surface current density through the following relation, namely

$$\vec{J} = \hat{n} \times \vec{H} \tag{22}$$

17

where $\hat{n}$ is the normal to the surface. Therefore, the total Fock current in the shadow region is given by

$$\vec{J}_E^S = -\hat{\phi} \, H_0 \{ e^{-j\beta\ell_1} g(\xi_1) + e^{-j\beta\ell_2} g(\xi_2) \} \tag{23}$$

where

$$\xi_1 = \left(\frac{\beta a}{2}\right)^{1/3} (2\pi - \phi), \text{ and}$$
$$\xi_2 = \left(\frac{\beta a}{2}\right)^{1/3} (\phi - \pi) \tag{24}$$

The computed results of the Fock current for the circular cylinder of radii equal to 0.2, 1.2 and 3.2 wavelengths are given in Figures 6, 7 and 8, respectively.

While the expressions given here are specifically valid for the circular cylinder, Fock theory is valid for all smooth bodies and for both TE and TM polarizations and may be used to obtain the shadow-side current in all such cases.
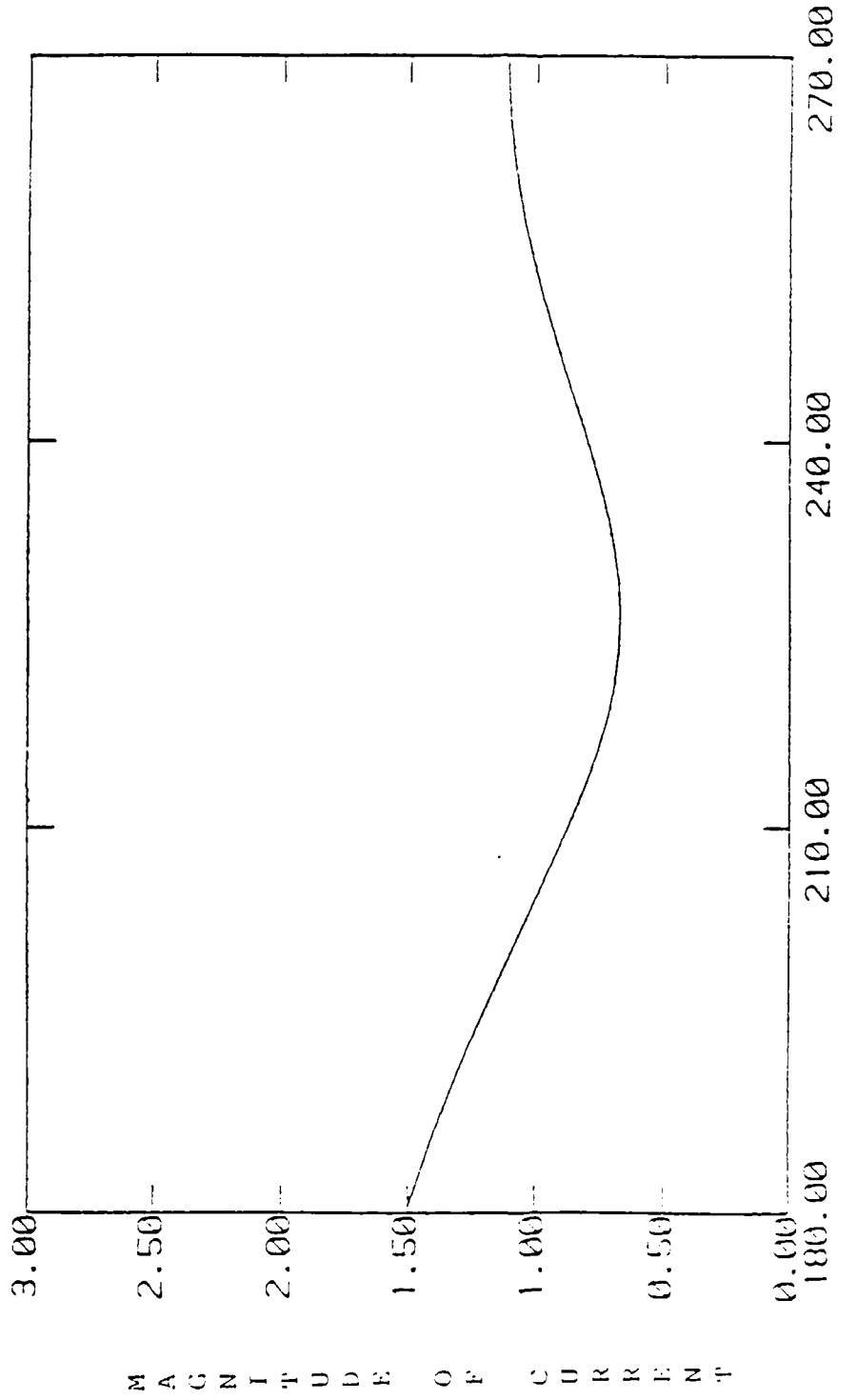
18

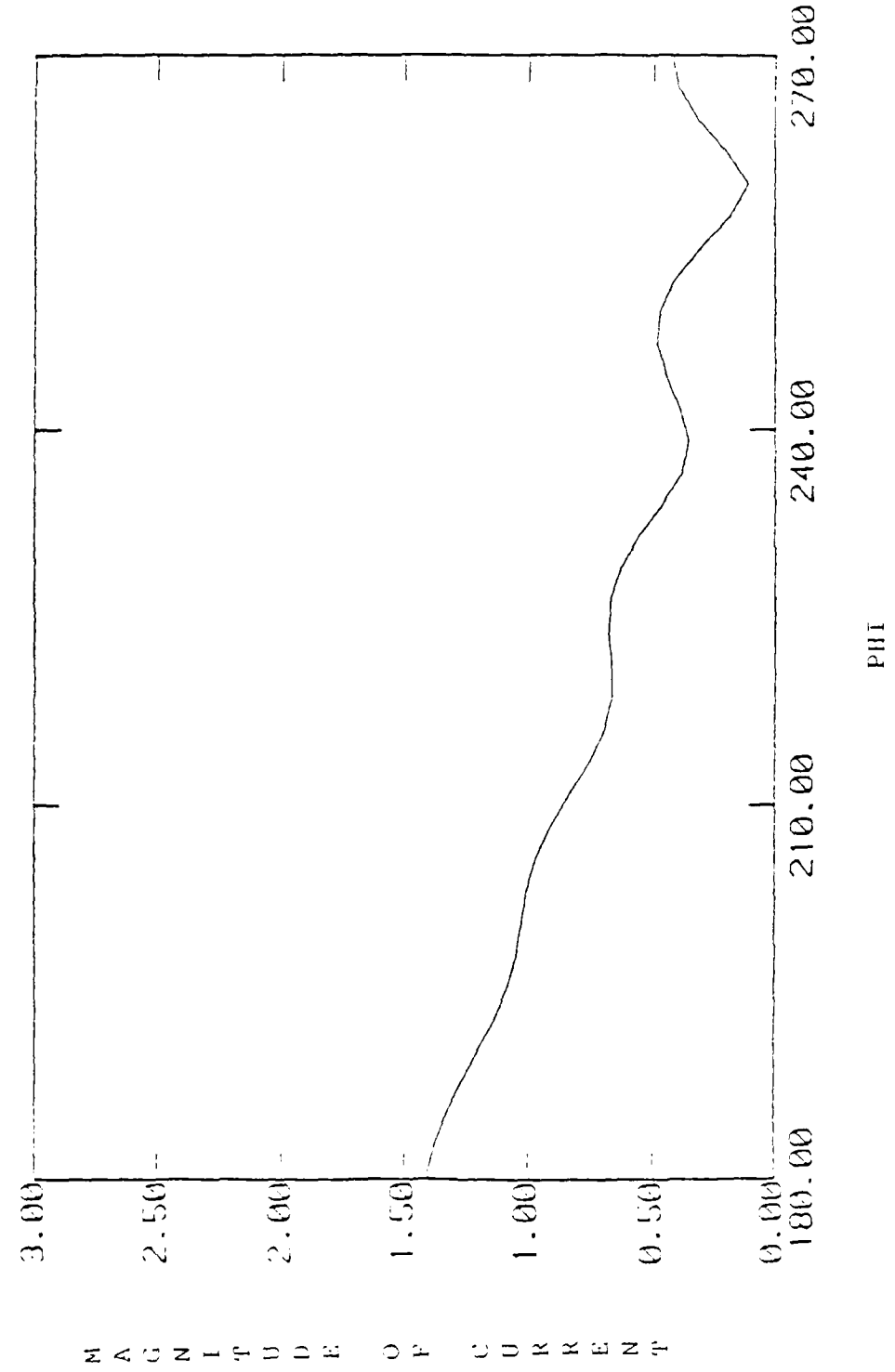Figure 6. Shadow-side Fock current on a circular cylinder of radius 0.2λ with $\phi_i = 90^0$.

Figure 7. Shadow-side Fock current on a circular cylinder of radius 1.2λ with $\phi_i = 90^0$.

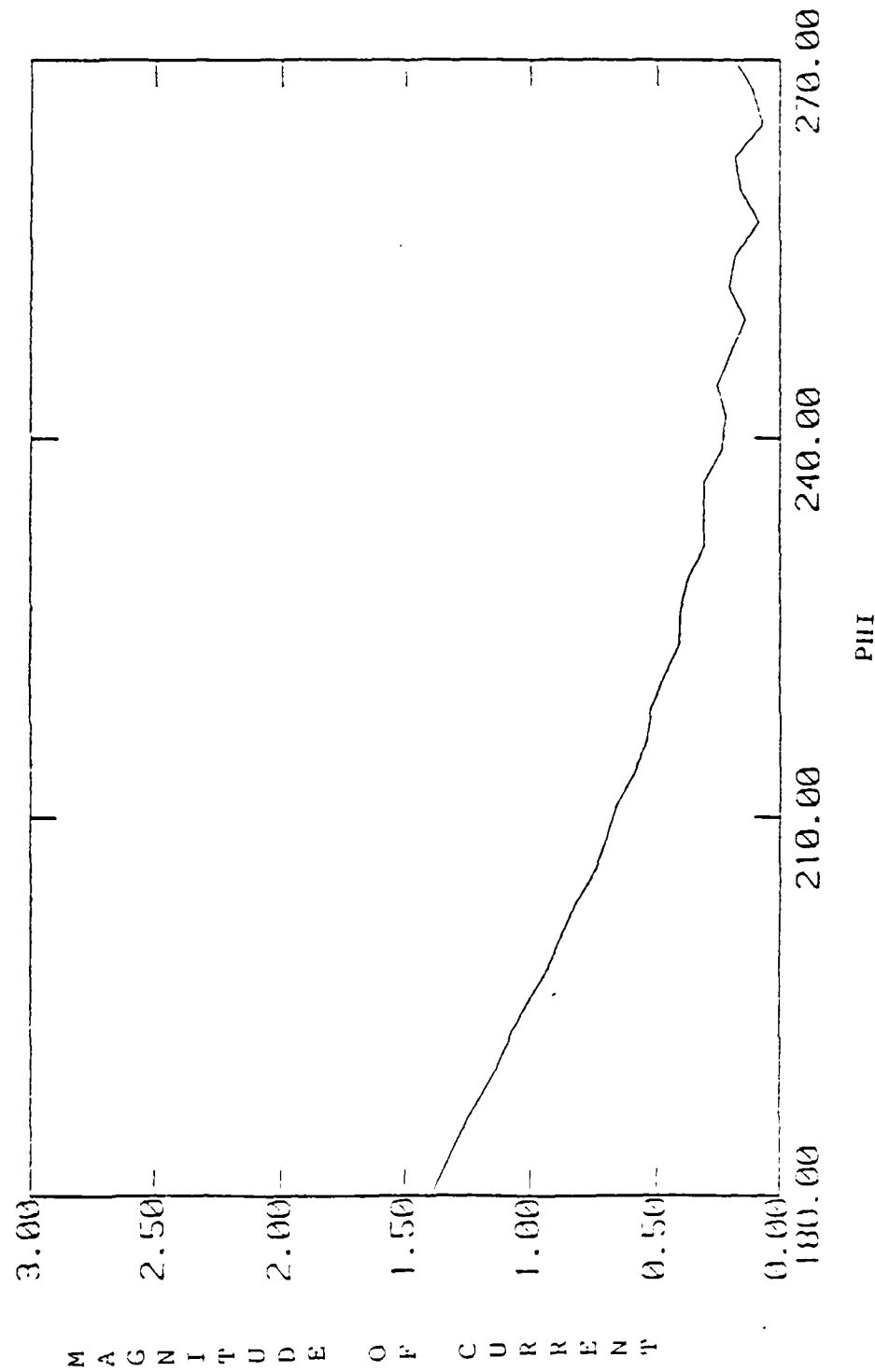Figure 8. Shadow-side Fock current on a circular cylinder of radius 3.2λ with $\phi_i = 90^0$.

21

IV. NUMERICAL CONSIDERATIONS

A. Surface Discontinuities

In evaluating the integrals during the iteration process, special attention has to be paid to surface discontinuities which, if not treated correctly, give rise to numerical errors. As an example, consider the wedge shown in Fig. 9. Here the edge of the wedge is the discontinuity. The current on face A is given by

$$\vec{J}^A(\ell) = 2\hat{n}x \; \vec{H}_i(\ell) + 2\hat{n}x \int_B \vec{J}^B(\ell')x \; \vec{\nabla}'G(r)d\ell' \; . \tag{25}$$

Introducing the Greens function as given in Eq. (4) and carrying out the vector products, this becomes:

$$J^A(\ell) = 2H_i(\ell) + \frac{j\beta}{2} \int_{\ell'=0}^{\infty} J^B(\ell') \; H_1^{(2)}(\beta r) \; \cos\psi d\ell' \; . \tag{26}$$

Then, for field points close to the edge ($\ell \to 0$) and source points close to the edge ($\ell' \to 0$), the distance r between them tends to zero and the Hankel function has the following small parameter behavior:

$$H_1^{(2)}(\beta r) \approx j \; \frac{2}{\pi\beta r} \; . \tag{27}$$

Under these conditions, the integrand contains an inverse distance function which gives rise to large error when integrated numerically. However, this integral can be evaluated analytically as follows. From Fig. 9, it can be seen that
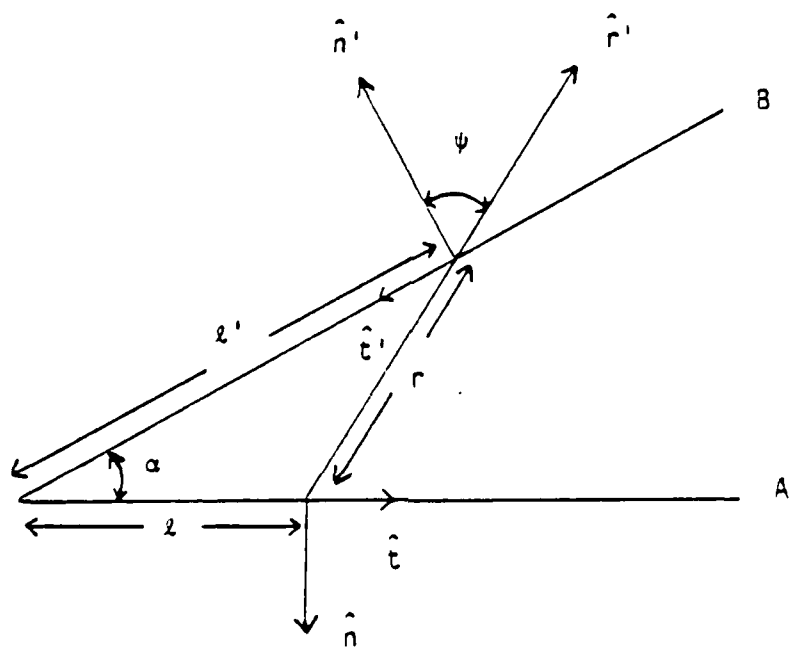
22

Figure 9. Geometry and definitions for edge current calculations.

$$\cos\psi = \frac{\ell}{r}\sin\alpha \tag{28}$$

and

$$r = \sqrt{{\ell'}^2 + \ell^2 - 2\ell\ell'\cos\alpha} \ \ . \tag{29}$$

Hence, for $\ell \to 0$ and $\ell' \nrightarrow 0$, $\cos\psi \approx 0$ so that for field points close to the edge source points far from the edge do not contribute to the integral in (28). The upper limit of integration can be replaced by a finite value, and Eq. (28) can be written with the aid of Eqs. (27) -(29) as follows:

$$J^A(\ell\to 0) = 2H^i(0) - J^B(\ell'\to 0)\frac{\ell\sin\alpha}{\pi}\int_0^L \frac{d\ell'}{{\ell'}^2 + \ell^2 - 2\ell'\ell\cos\alpha} \ \ . \tag{30}$$

This is a standard integral which yields the following result:

$$J^A(\ell\to 0) = 2H^i(0) - J^B(\ell'\to 0)\left(\frac{\pi - \alpha}{\pi}\right) \ . \tag{31}$$

This result is general and holds for the optics and correction currents alike. Its importance lies in the fact that the edges of polygonal structures and edge-like protrusions on surfaces do not have to be truncated, as was done in [8], or dealt with using a different approach. Hence, the current at the edge can be computed without the need for resorting to a hybrid approach.

24

B. CONVEX SURFACES

For surfaces comprised of planar sections, the term $2\hat{n} \times L[\vec{J}]$ in the MFIE is identically zero for observation and integration points on the same planar section. This, however, is not true for convex surfaces, in which case the integrals are singular due to the singular behavior of the Greens function and, hence, principle value integrals have to be used.

The details of the principle value calculation for the three-dimensional case are given in [9], with the result that

$$\int_{\Sigma} \vec{J}(\vec{R}') \times \vec{\nabla}' \, G(r) \, ds' = \int_{\Sigma'} \vec{J}(\vec{R}') \times \vec{\nabla}' \, G(r) \, ds' - \frac{\vec{J}(\vec{R})}{2\pi} [4\pi - \Omega] \qquad (32)$$

where $\Sigma' = \Sigma - \varepsilon$, ε being the neighborhood of the singularity. Ω is the absolute value of the solid angle subtended by the deformed surface (in taking $\int$) at the field point $\vec{R}$, and has to be determined from the geometry of the surface. If Σ is smooth at $\vec{R}$, then $\Omega = 2\pi$.

For the two-dimensional case, it will be shown that the integral in the MFIE remains finite despite the singularity in the Greens function. Consider, for example, the case of a cylinder of circular cross section as shown in Fig. 5. For this two-dimensional scattering problem, Eq. (7) is given by:

$$L[\vec{J}] = \hat{t}' \int_{\ell'} K(\vec{R}, \vec{R}') \, J(\ell') d\ell' \qquad (33)$$

where

$$K(\vec{R}, \vec{R}') = \frac{j\beta}{2} (\hat{n}' \cdot \hat{r}') \, H_1^{(2)}(\beta r) \qquad (34)$$

25

and $\hat{t}'$ is the direction of the current at the source point P'. Using Fig. 5, it can be shown that

$$\hat{n}' \cdot \hat{r}' = \sin \frac{|\phi' - \phi|}{2} = \frac{r}{2a} \tag{35}$$

Substituting Eqs. (35) and (37) in (34), we find that

$$K(\vec{R}, \vec{R}') \underset{r \to 0}{\to} - \frac{1}{2\pi a} \tag{36}$$

and therefore $L[\vec{J}]$ will be finite for any two-dimensional scattering problem.

26

V. NUMERICAL EXAMPLES

In this section, we illustrate the technique described in earlier sections. We deal with scatterers with surface discontinuities as well as smooth surfaces. Scatterers with edges are exemplified by a square cylinder. Scatterers with smooth surfaces are exemplified by circular and elliptic cylinders. In all cases discussed, the incident wave is a Transverse-Electric (TE) plane wave. Work on the Transverse-Magnetic (TM) case is partially done and will be the subject of another report in the near future.

A. SQUARE CYLINDER

Two examples are presented here. In both cases, the size of the cylinder is the same, viz., $w = 3.7\lambda$. However, the angles of incidence, ϕ_i, are different. The case, $\phi_i = 115^0$, has been dealt with in an earlier report [3]. We study the same case here using our hybrid-iterative technique. It was necessary in [3] to compute four orders of correction currents to obtain a sufficiently accurate result. With the hybrid iterative technique, zeroth order optics currents themselves give a sufficiently accurate solution. We also present the first-order optics currents for comparison. Figures 10 to 14 show the results for $w = 3.7\lambda$ and $\phi_i = 115^0$.

We also consider the case when $\phi_i = 95^0$. Note that in this case, Face 2 of the square cylinder is almost, but not quite, in the visible region. As can be seen from the final result, the current on this is quite appreciable
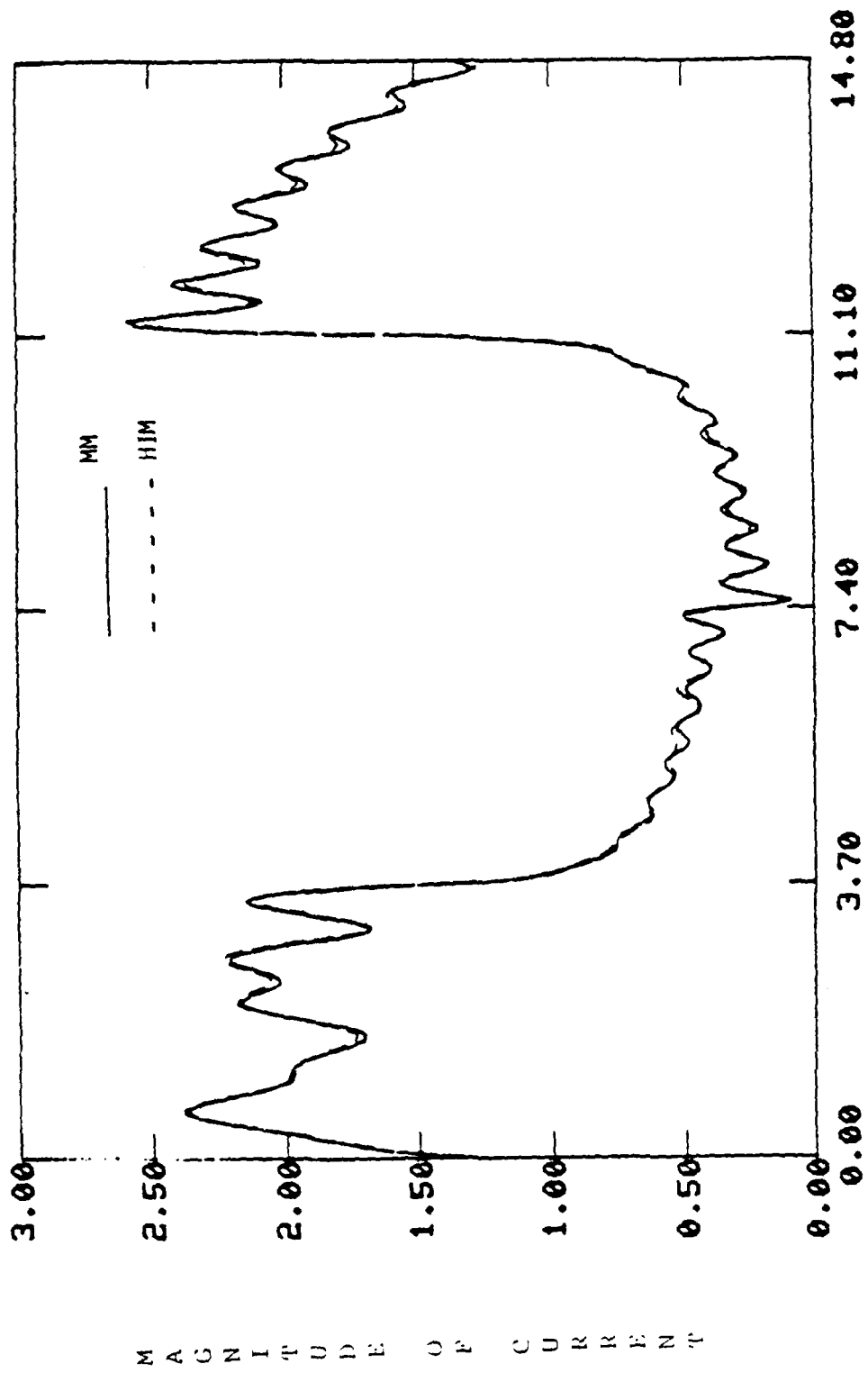
Figure 10. Magnitude of current on square cylinder. Order = 0.
w = 3.7λ, ψ_i = 115°. MM = Moment Method, HIM= Hybrid iterative method.
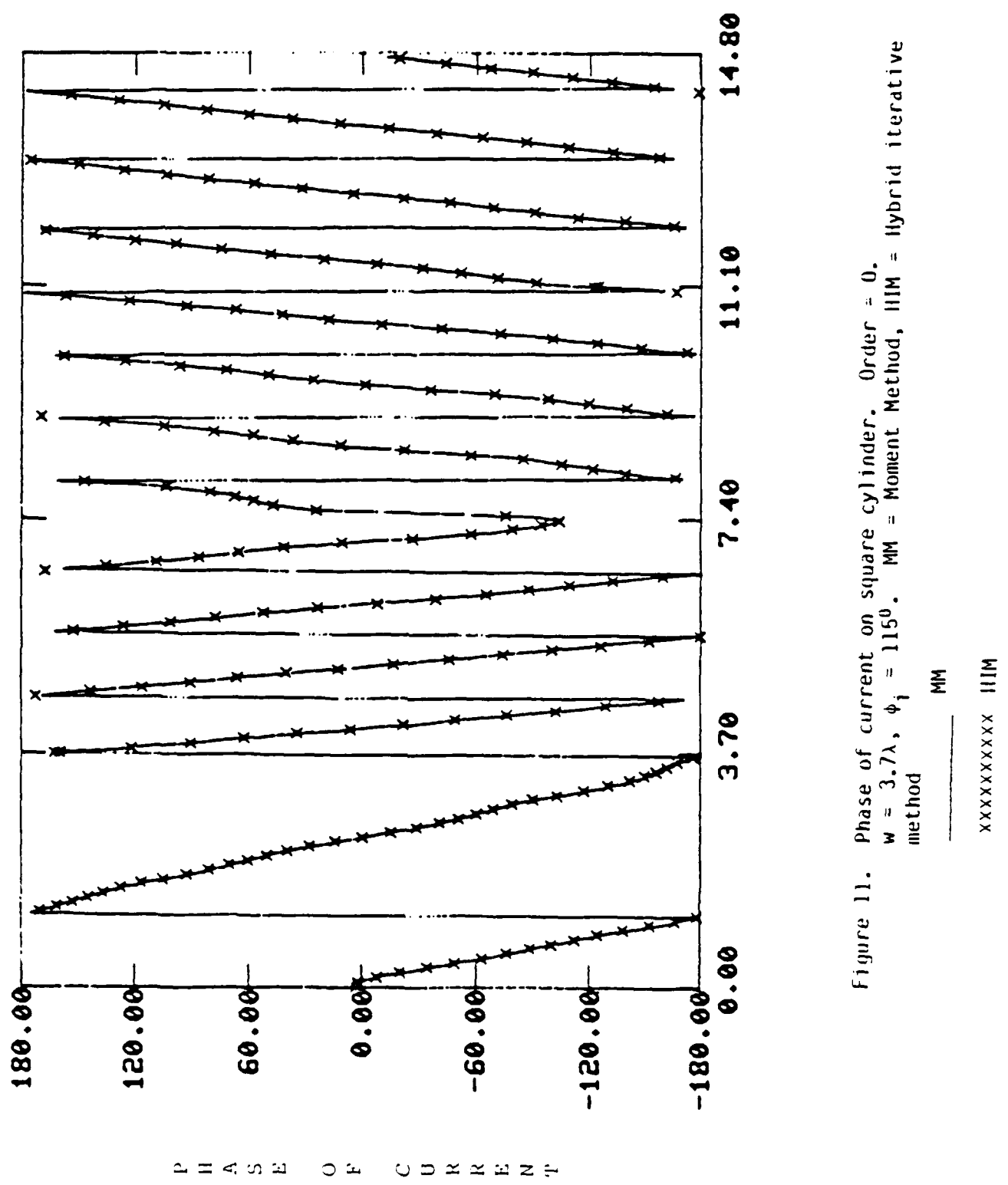
Figure 11. Phase of current on square cylinder. Order = 0.
w = 3.7λ, ϕ_i = 115⁰. MM = Moment Method, HIM = Hybrid iterative method

_____ MM

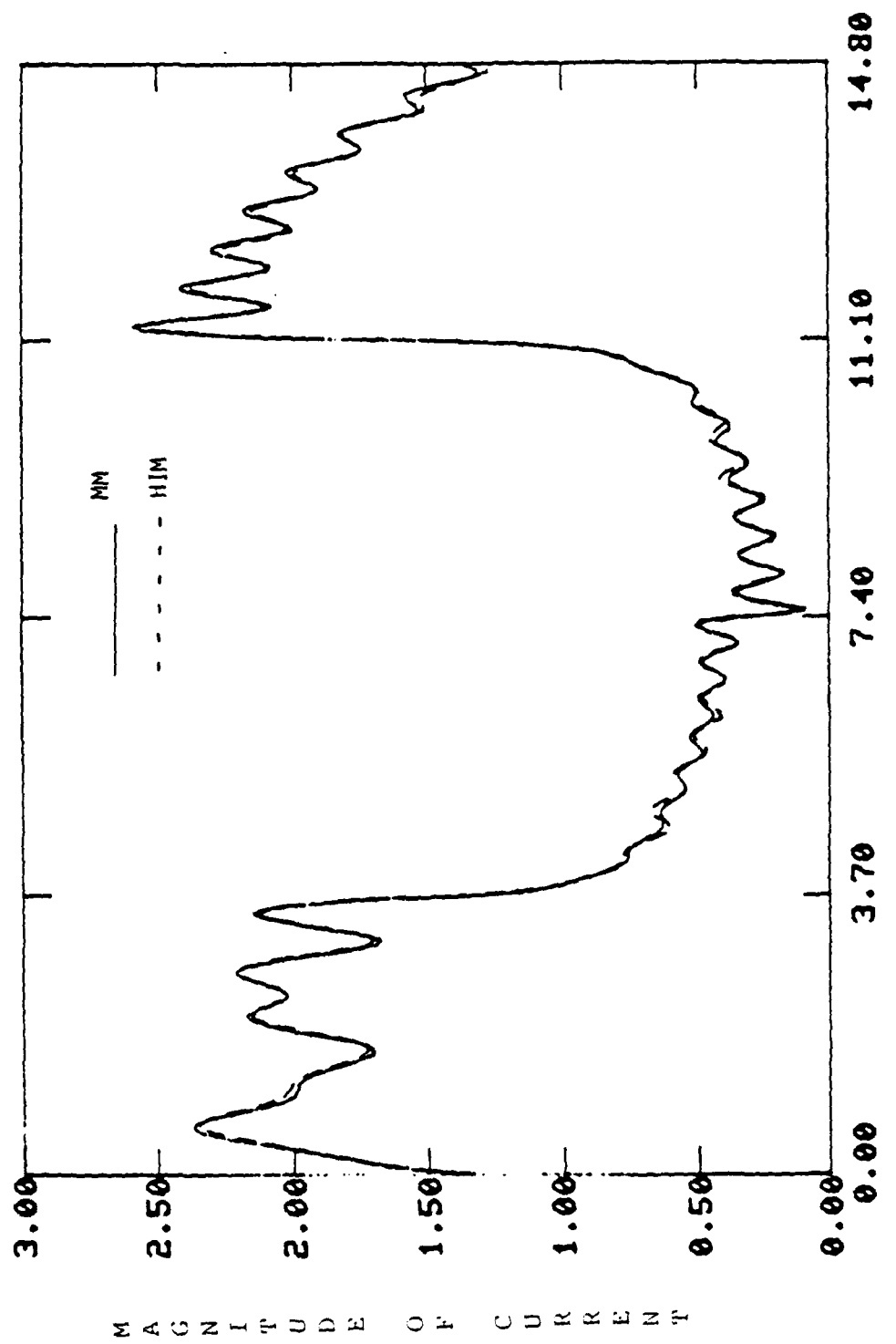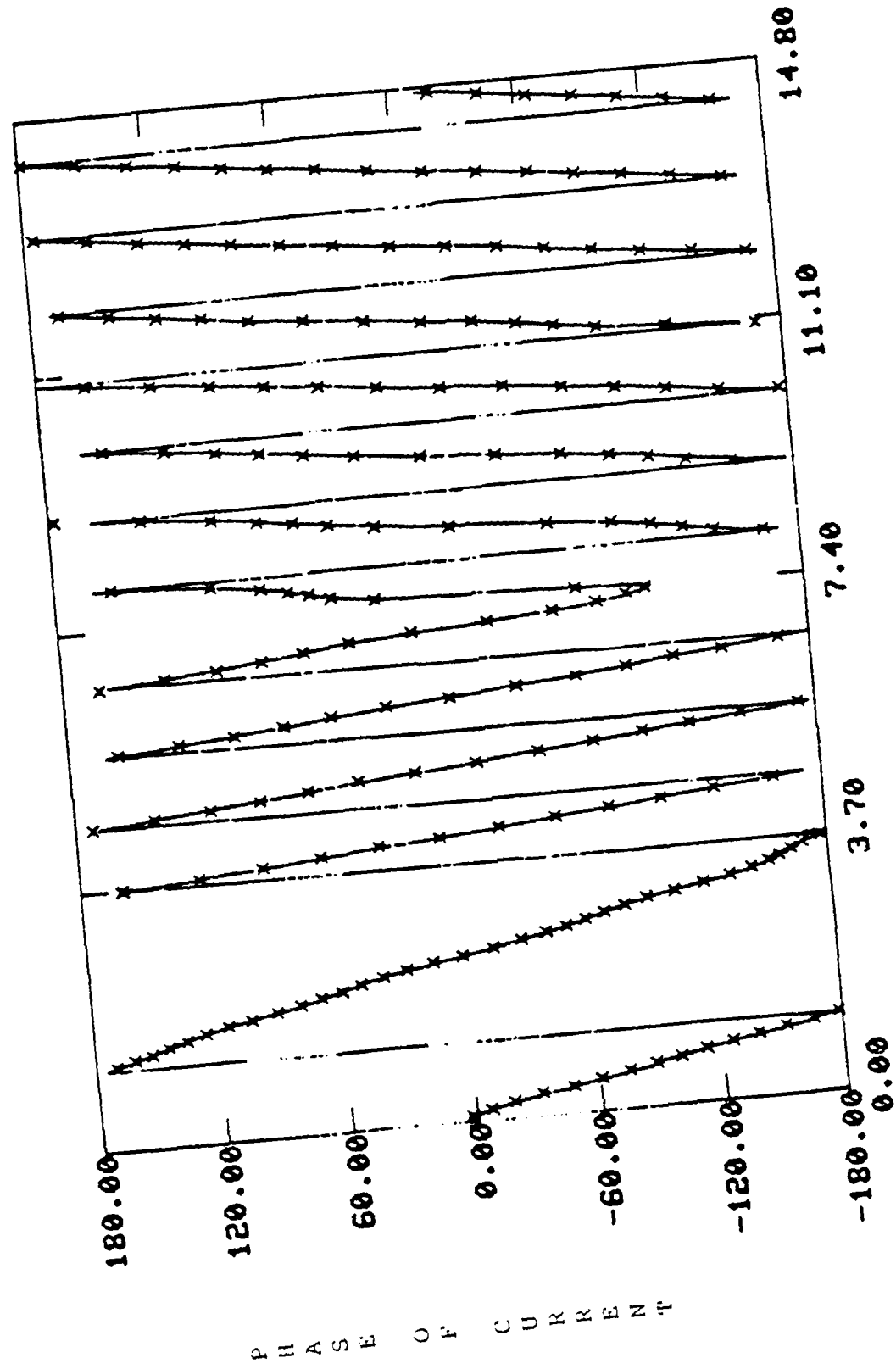xxxxxxxxx HIM

29

Figure 12. Magnitude of current on square cylinder. Order = 1.
w = 3.7λ, φ_i = 115°. MM = Moment Method, HIM = Hybrid iterative
method

30

Figure 13. Phase of current on square cylinder. Order = 1.
$w = 3.7\lambda$, $\phi_i = 115^0$. MM = Moment Method, HIM = Hybrid iterative
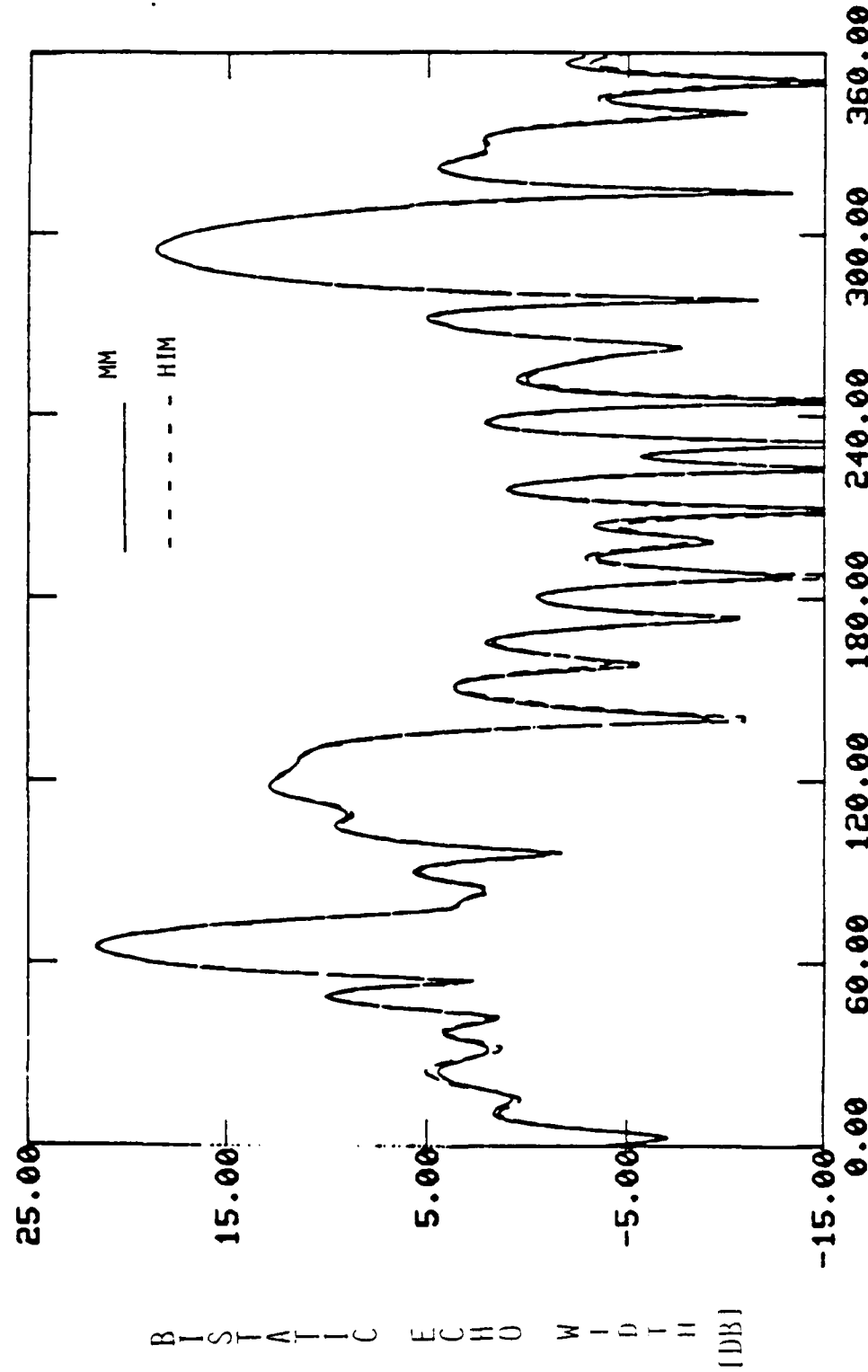method

——————— MM

xxxxxxxxxx HIM

Figure 14. Bistatic echo width of a square cylinder. Order = 1.
$w = 3.7\lambda$, $\psi_1 = 115^0$. MM = Moment Method, HIM = Hybrid iterative method.

32

and may not be neglected initially as was done in the iterative technique. Figures 15-19 show results corresponding to this case. In this case it was necessary to compute up to the second-order optics currents.

B. SCATTERERS WITH SMOOTH SURFACE

i) Circular Cylinder:

In [2], Kaye, Murthy and Thiele used the iterative technique to compute the surface currents on a circular cylinder of radius 3.2λ. These computations include the first-order correction current and are characterized by a ripple. For the same cylinder, we computed induced currents using the hybrid-iterative technique. These results are presented in Figures 20-22. Note that there is no ripple and that the agreement between our results and the exact eigenfunction solution is excellent. Furthermore, we needed to compute only up to the zeroth-order optics currents.

In order to demonstrate that our technique works well for "small" bodies, we also consider a 0.2λ radius circular cylinder. We compute both zeroth-order and first-order optics currents. These results are shown in Figures 23-27. Note the excellent agreement between our results and the exact results obtained using the eigenfunction solution.

The computer code we have written is general and may be used to compute the induced currents on scatterers with an arbitrary cross-section. To demonstrate this generality, we have also considered an elliptic cylinder (Figure 28) with semi-major and semi-minor axes being 1.5λ and 1.0λ, respectively. Our results are compared with those of the method of moments (MM). These results are shown in Figure 29-31. Note the excellent agreement between the results obtained from the MM and hybrid-iterative technique.
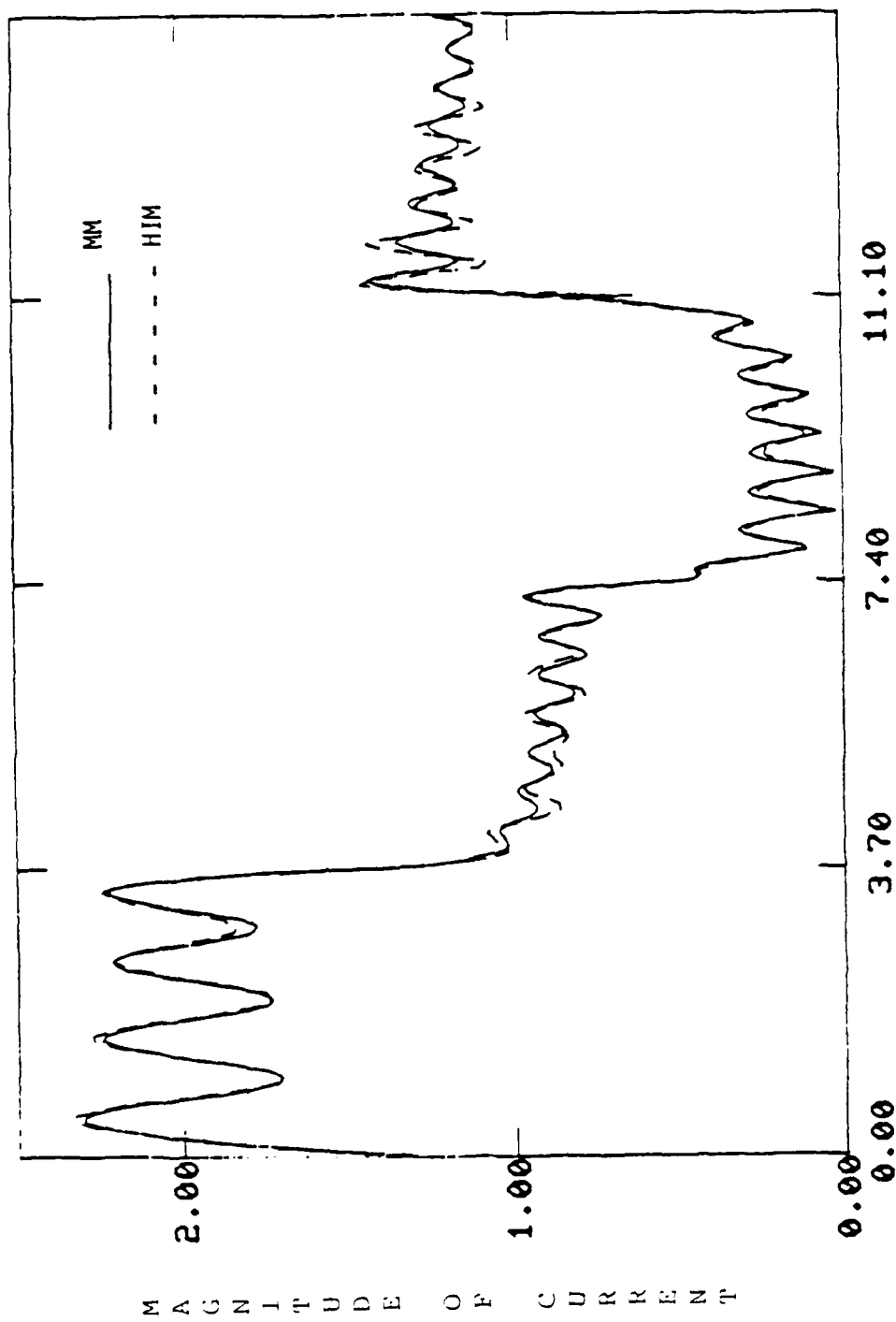
Figure 15. Magnitude of current on square cylinder. Order = 0. w = 3.7λ, ϕ_i = 95⁰ . MM = Moment Method, HIM = Hybrid iterative method.

34

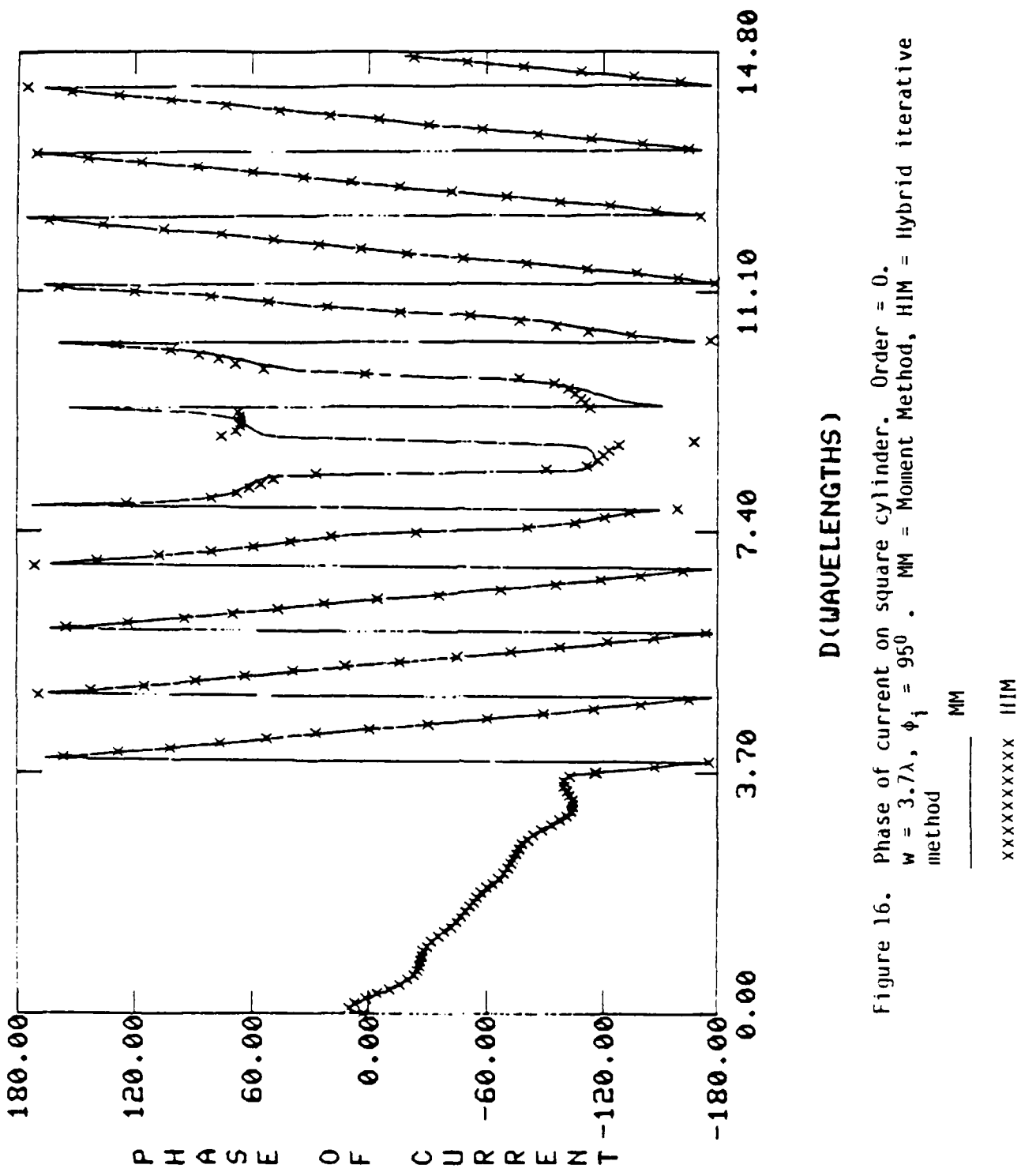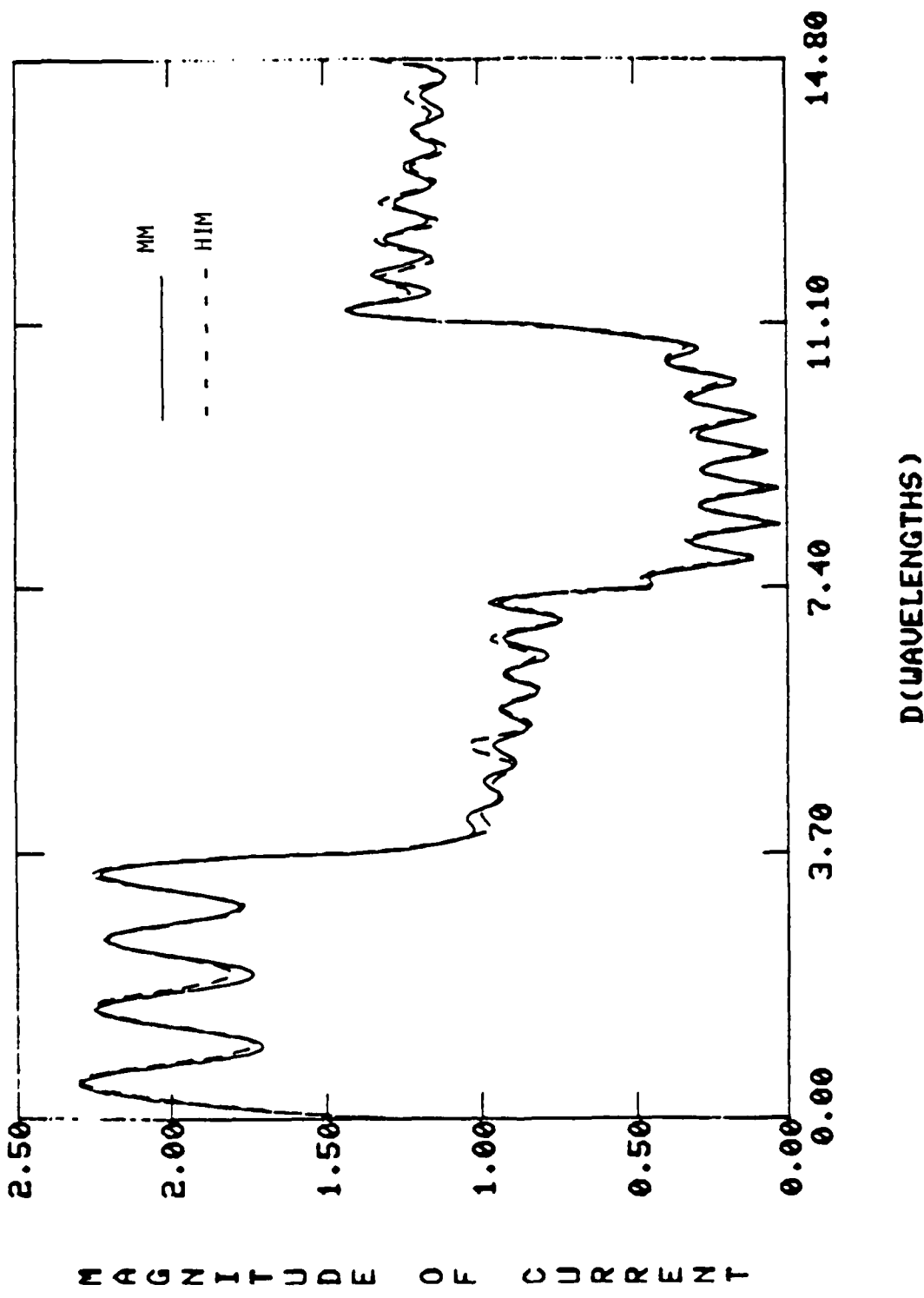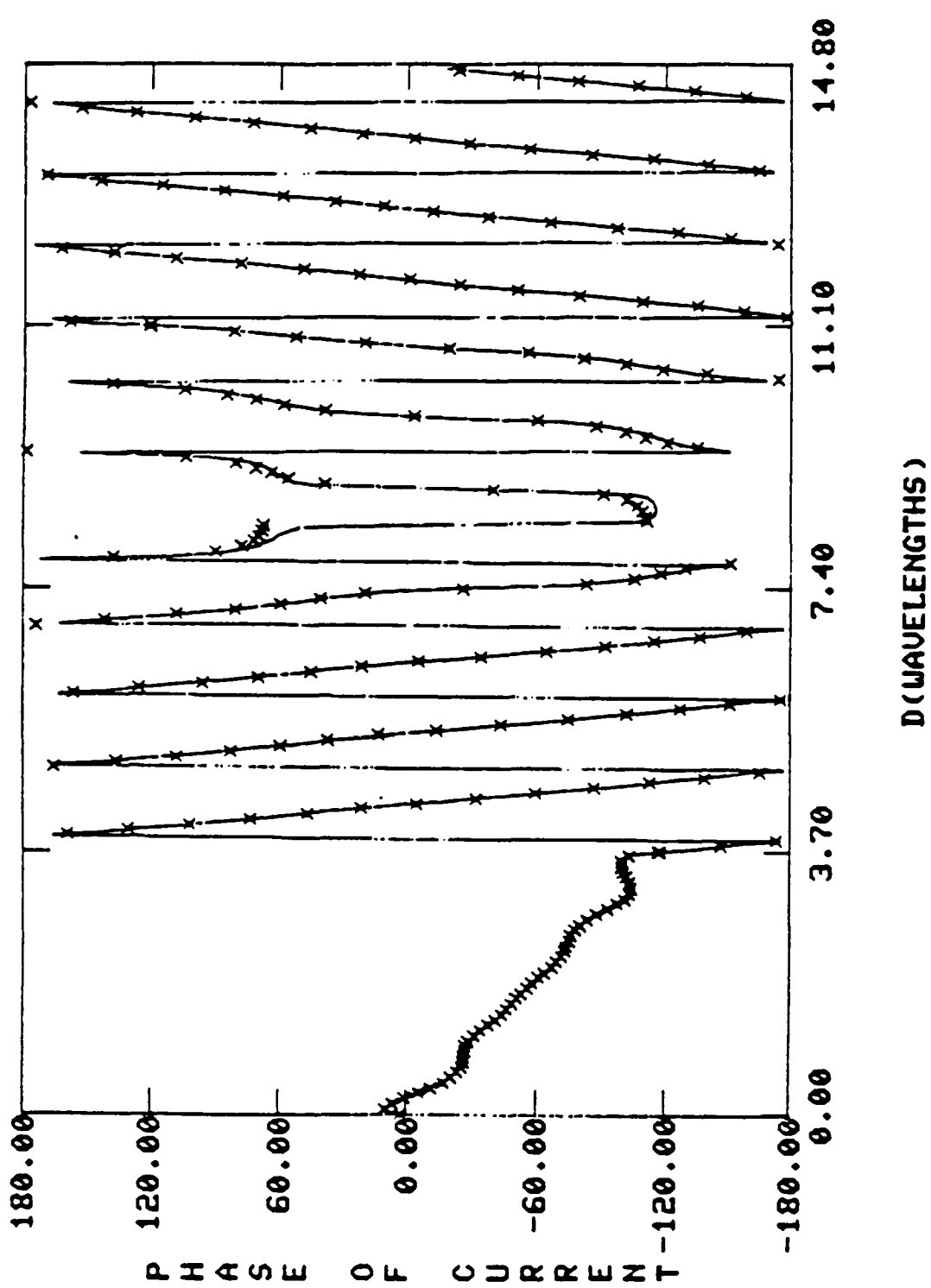Figure 16. Phase of current on square cylinder. Order = 0.
w = 3.7λ, φ_i = 95⁰ . MM = Moment Method, HIM = Hybrid iterative
method

_____ MM

xxxxxxxxx HIM

35

Figure 17. Magnitude of current on square cylinder. Order = 2. w = 3.7λ, ϕ_i = 95°. MM = Moment Method, HIM = Hybrid iterative method

Figure 18. Phase of current on square cylinder. Order = 2.
w = 3.7λ, ψ_i = 95° . MM = Moment Method, HIM = Hybrid iterative
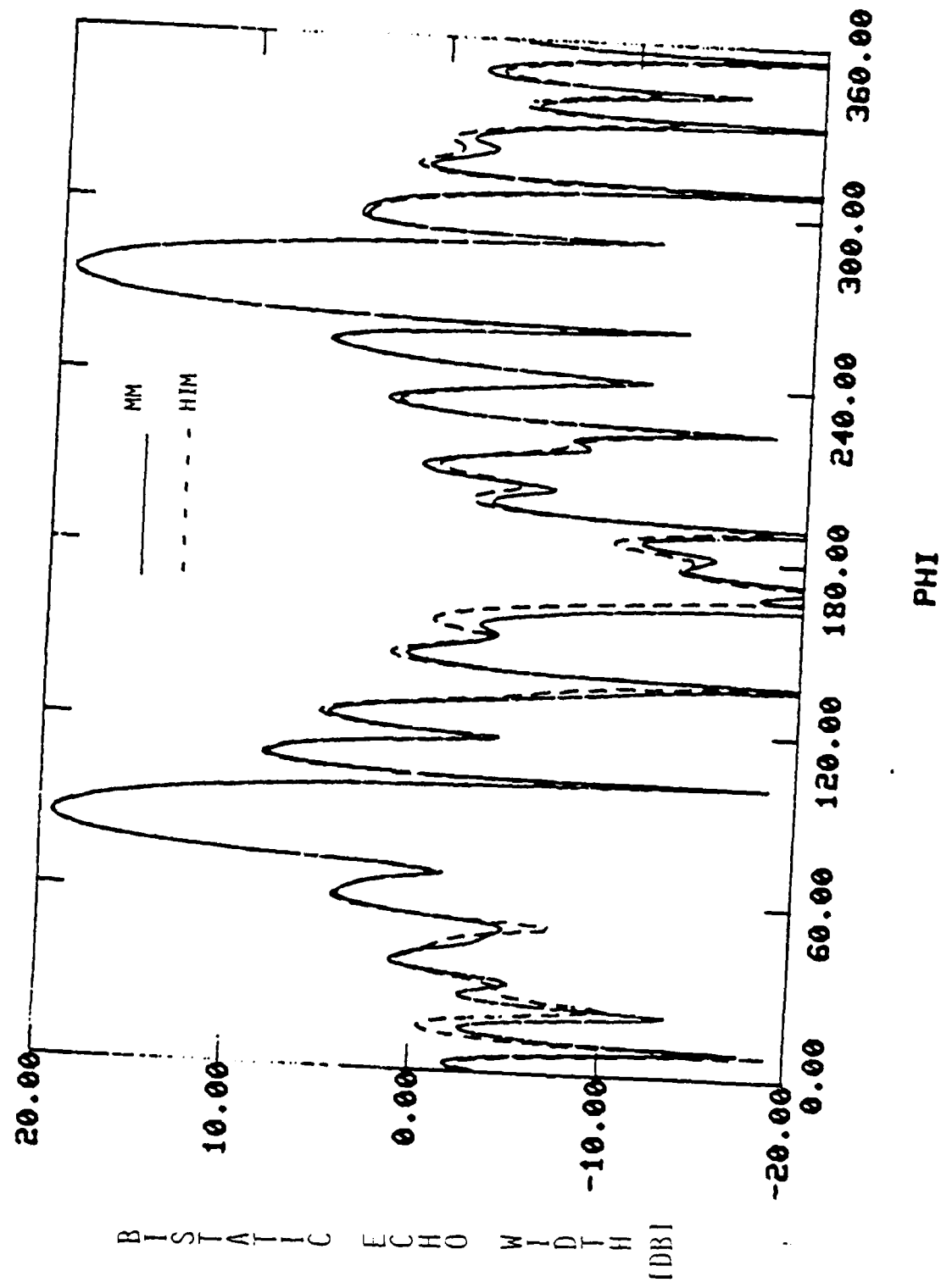method

————— MM

– – – – – HIM

37

Figure 19. Bistatic echo width of a square cylinder. Order = 2.
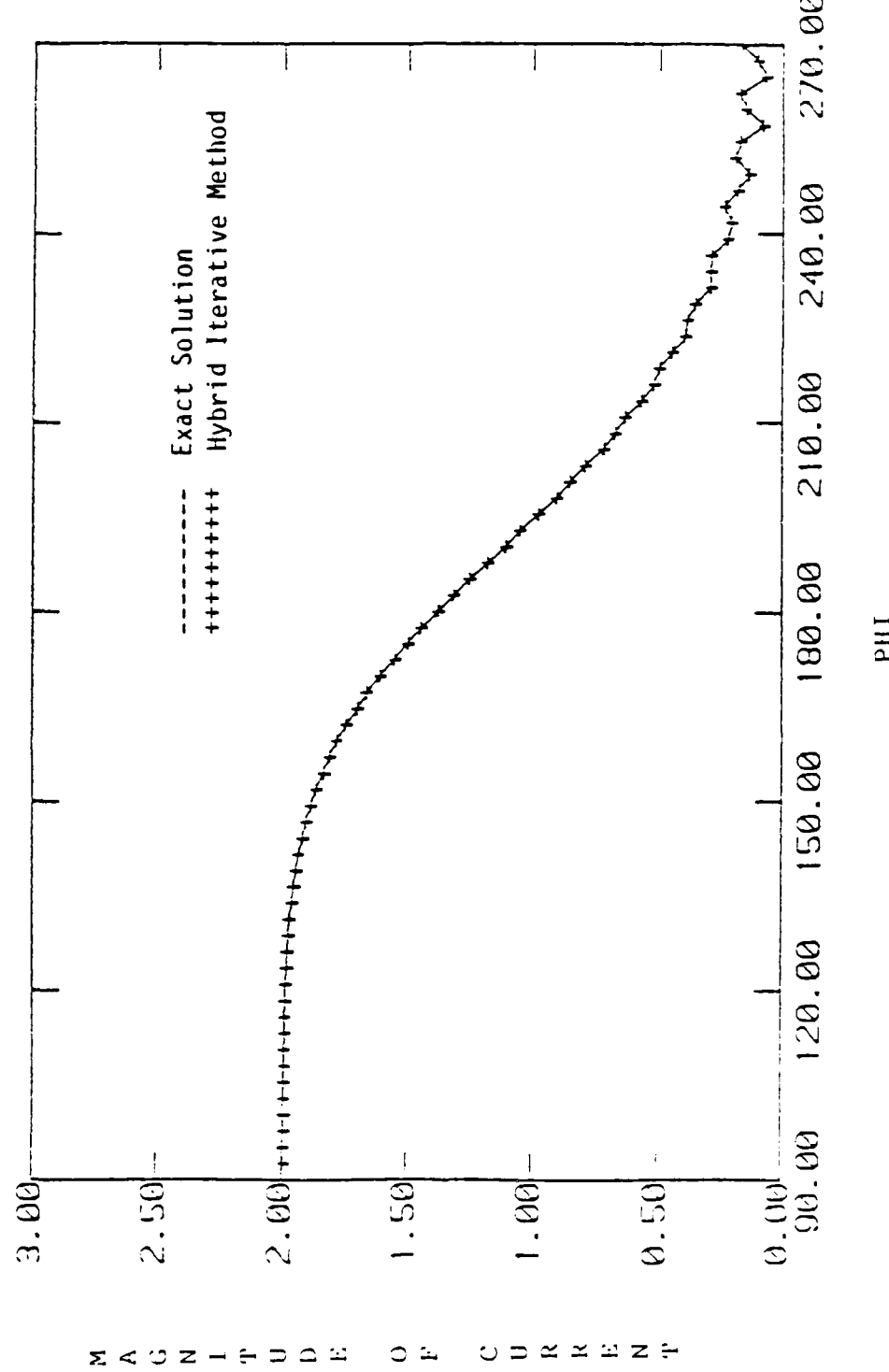$w = 3.7\lambda$, $\psi_i = 95^0$. MM = Moment Method, HIM = Hybrid iterative
method.

38

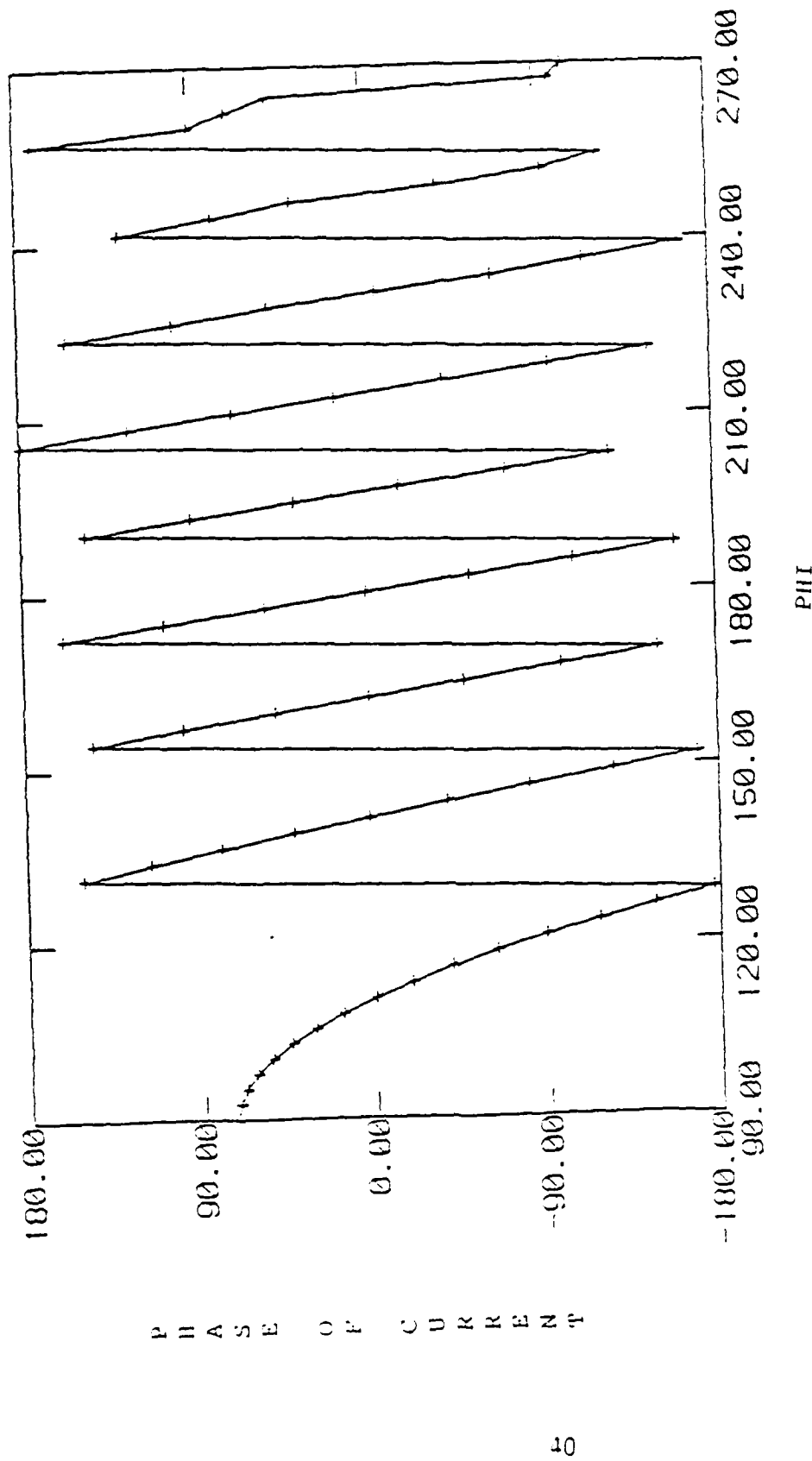Figure 20. Magnitude of zero-order optics current on a circular cylinder of radius 3.2λ with $\psi_i = 90^0$.

PHI

MAGNITUDE OF CURRENT

3.00
2.50
2.00
1.50
1.00
0.50
0.00

90.00   120.00   150.00   180.00   210.00   240.00   270.00

———— Exact Solution
++++++++++ Hybrid Iterative Method

Figure 21. Phase of zero-order optics current on a circular cylinder of radius 3.2λ with $\varphi_i = 90^0$.

Exact Solution
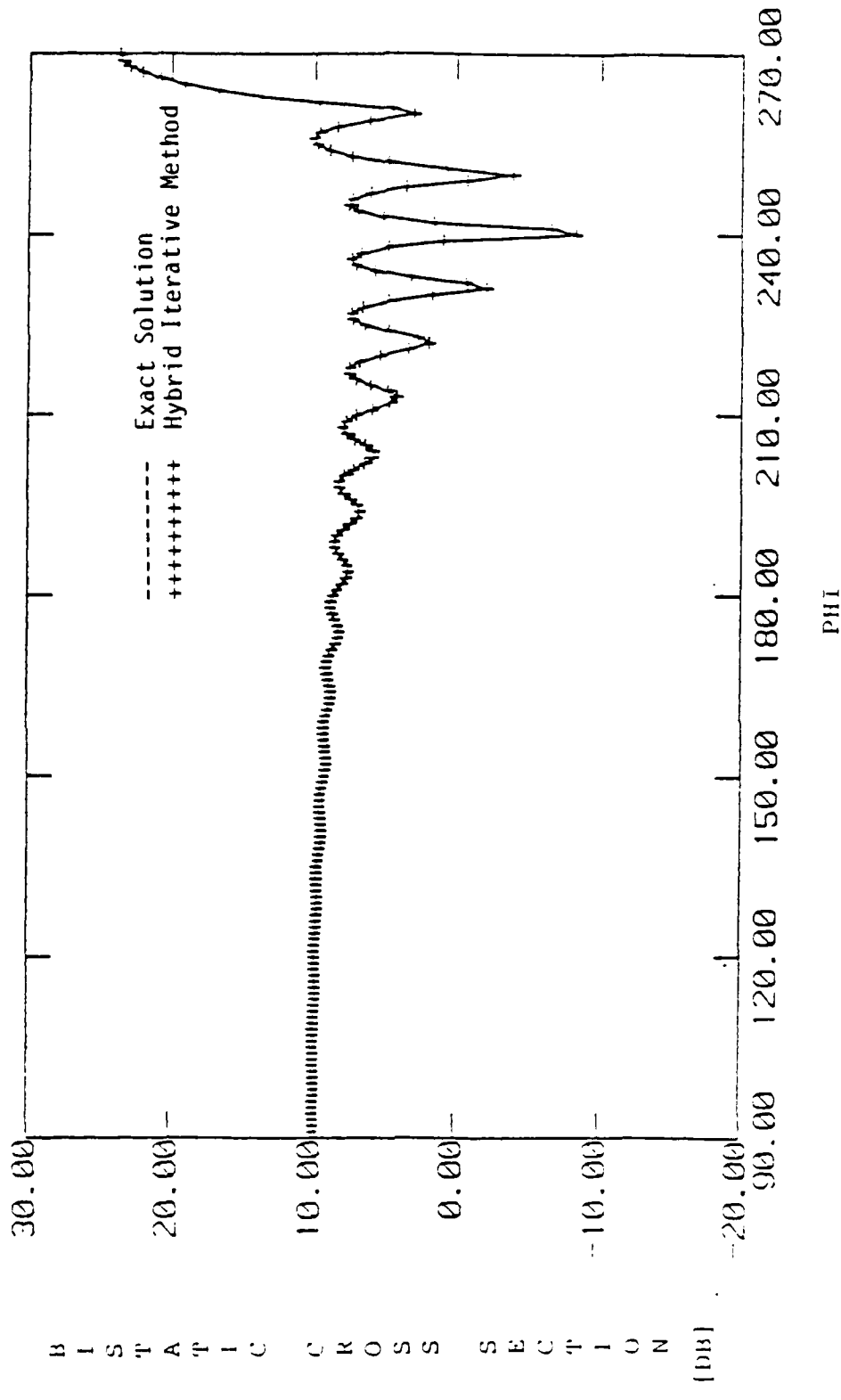++++++++++ Hybrid Iterative Method

40

Figure 22. Bistatic scattering pattern for a circular cylinder of radius 3.2λ with $\phi_i = 90^0$.
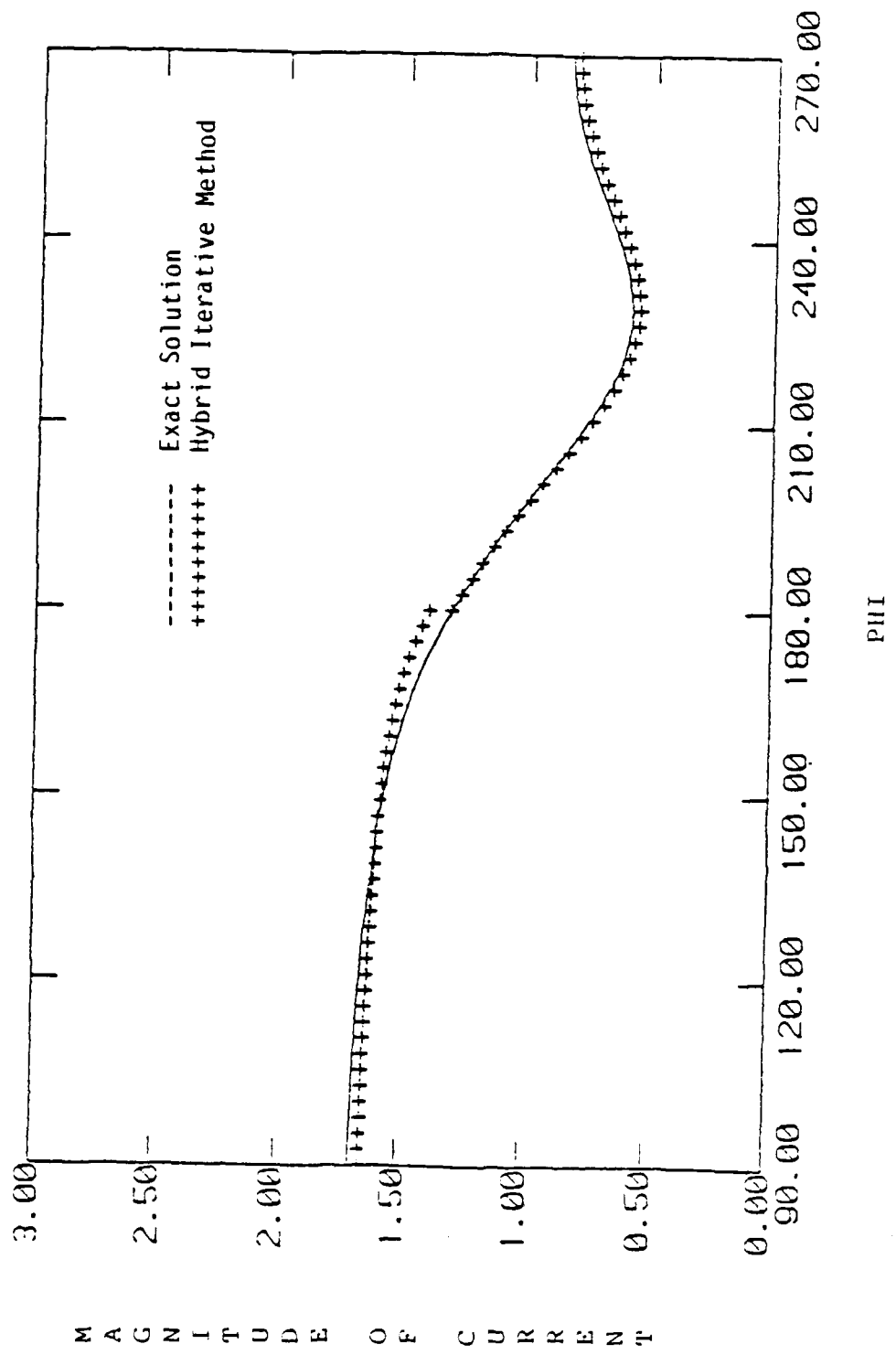
Figure 23. Magnitude of zero-order optics current on a circular cylinder of radius 0.2λ with $\phi_i = 90^0$.
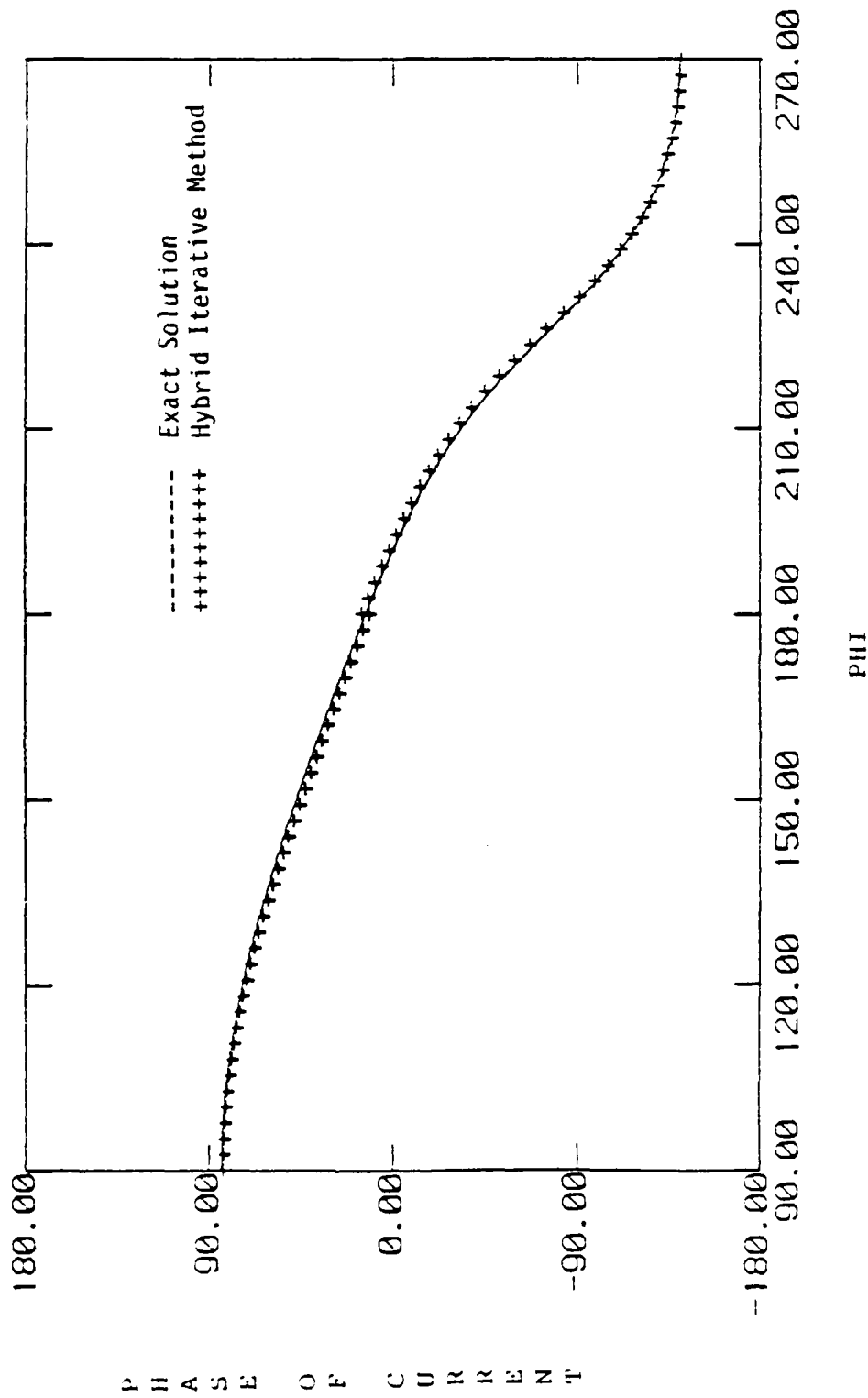
Figure 24. Phase of zero-order optics current on a circular cylinder of radius 0.2λ with $\phi_i = 90^0$.
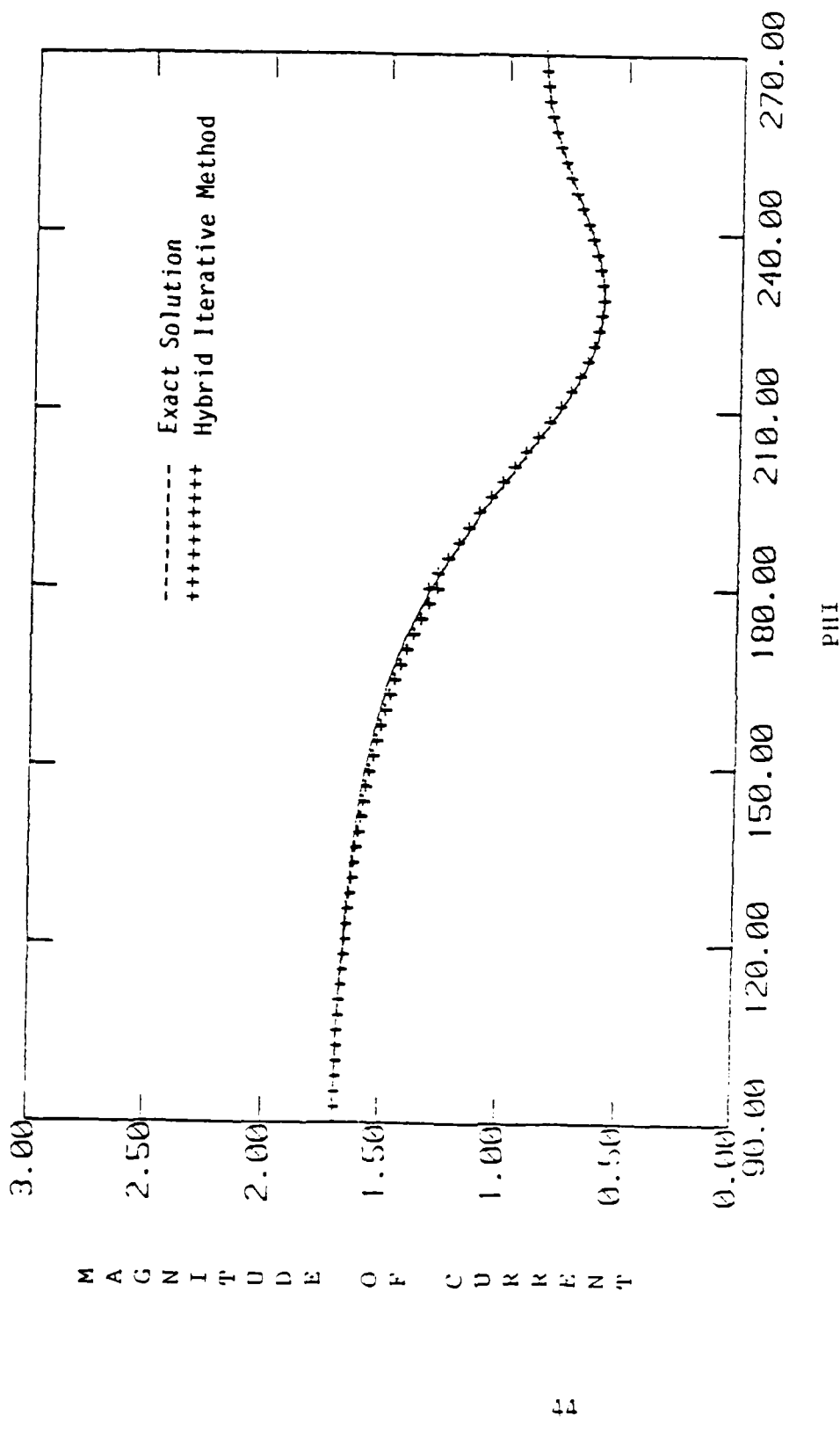
Figure 25. Magnitude of first-order optics current on a circular cylinder of radius 0.2λ with $\phi_i = 90^0$.
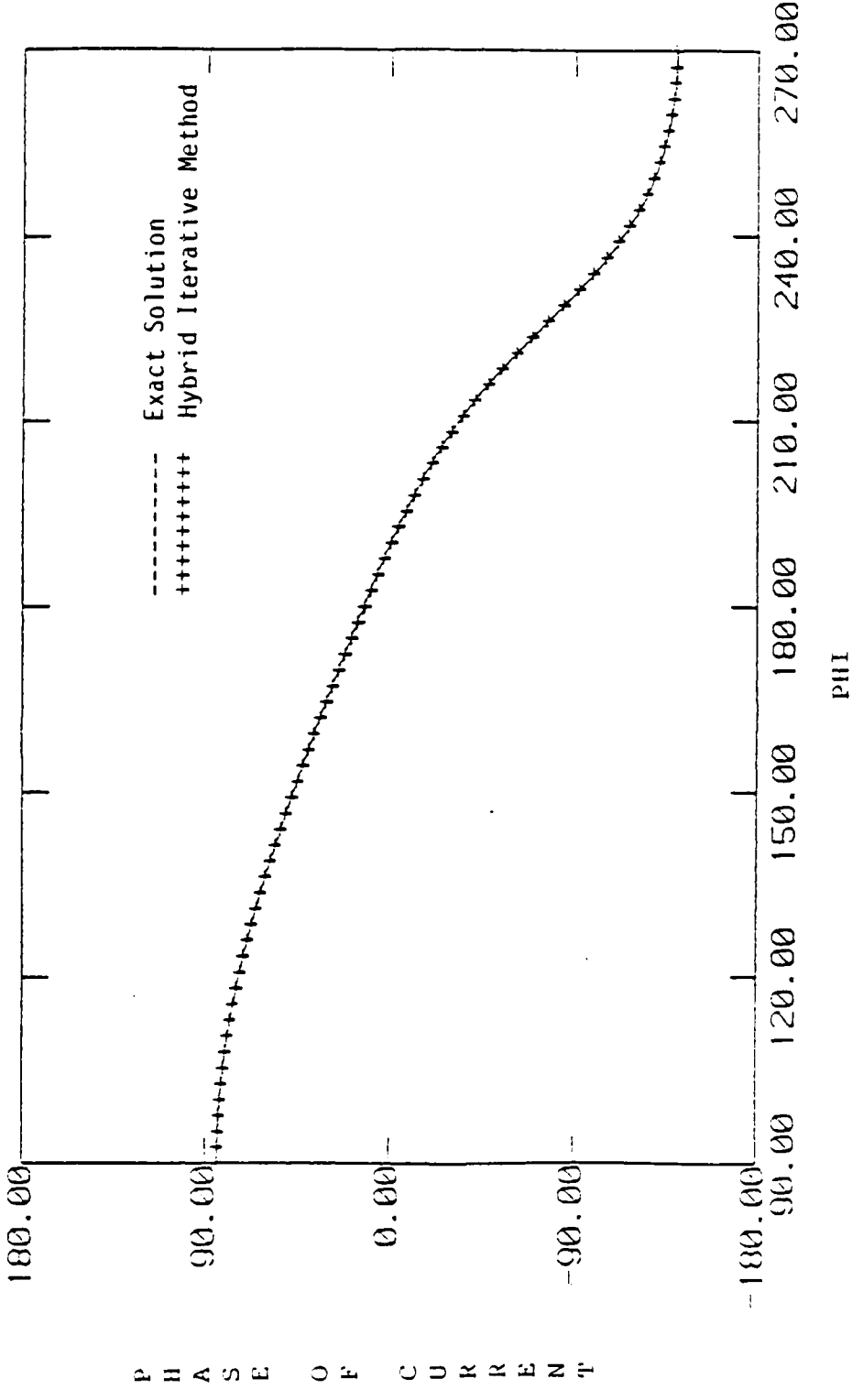
Figure 26. Phase of first-order optics current on a circular cylinder of radius 0.2λ with $\phi_i = 90^0$.

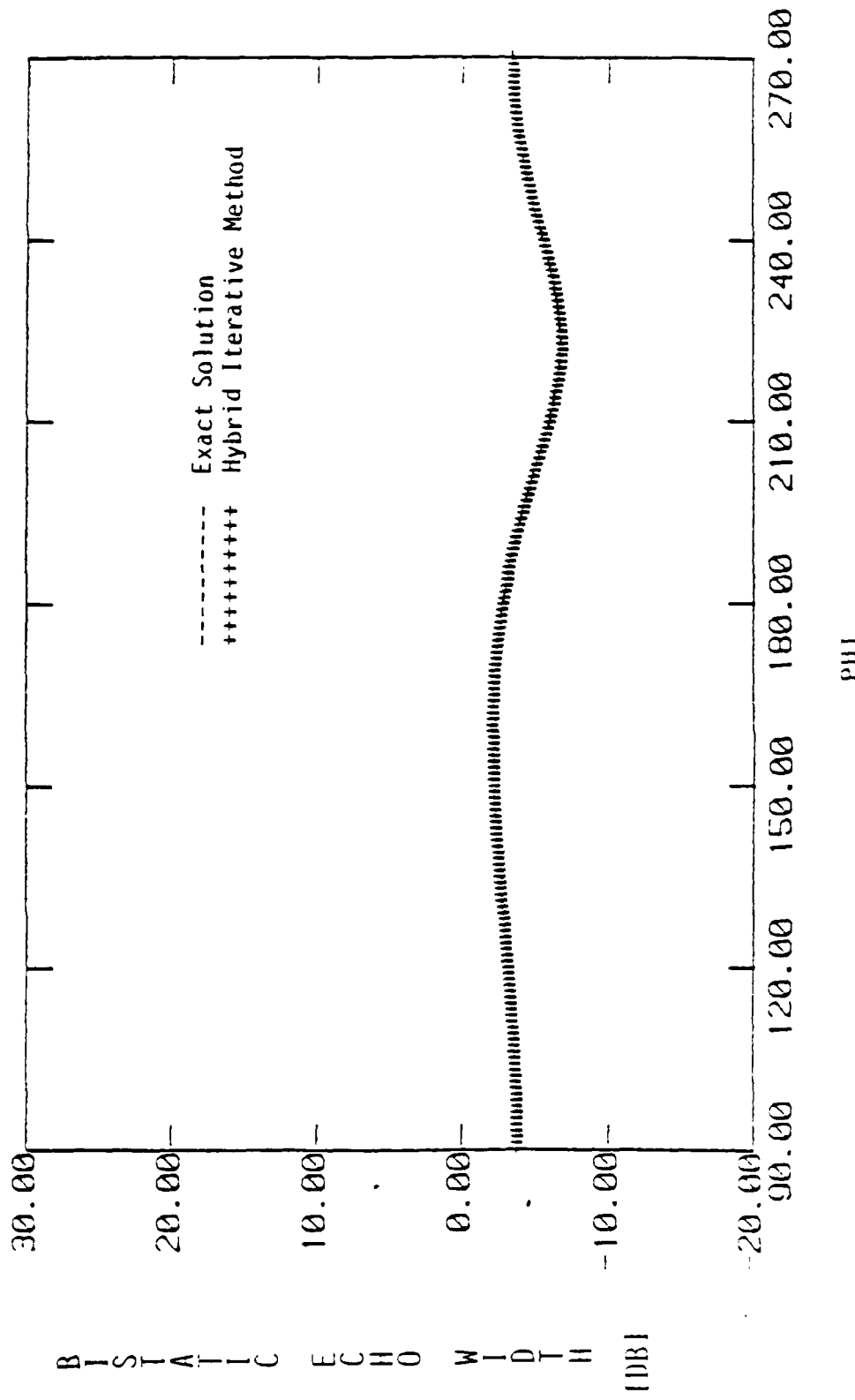Figure 27. Bistatic scattering pattern for a circular cylinder of radius 0.2λ with $\phi_i = 90^0$.

46
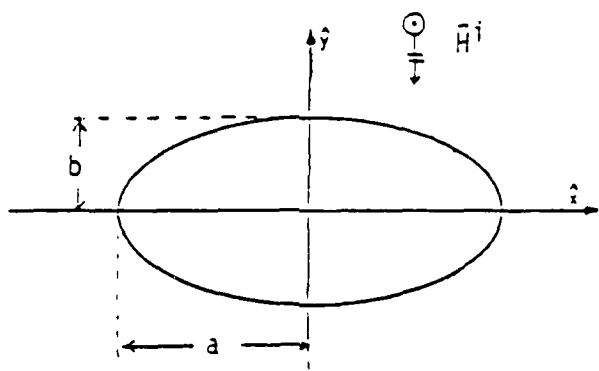
Figure 28. Geometry for the elliptic cylinder of semi-major axis "a" and semi-minor axis "b". Angle of incident plane wave is equal to 90 degrees.

47
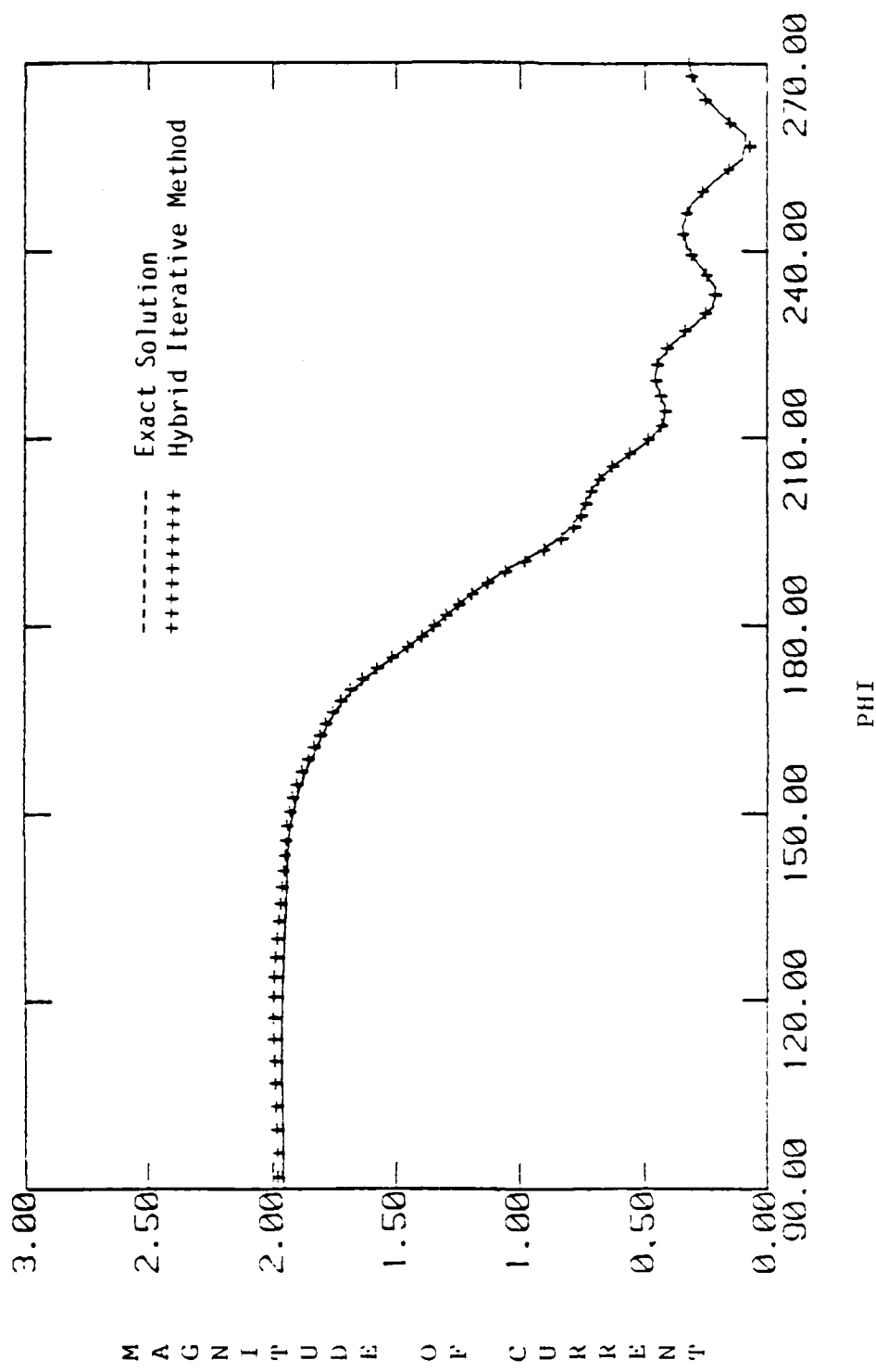
Figure 29. Magnitude of zero-order optics current on an elliptic cylinder of $a = 1.5\lambda$ and $b = 1.0\lambda$ with $\phi_i = 90°$.
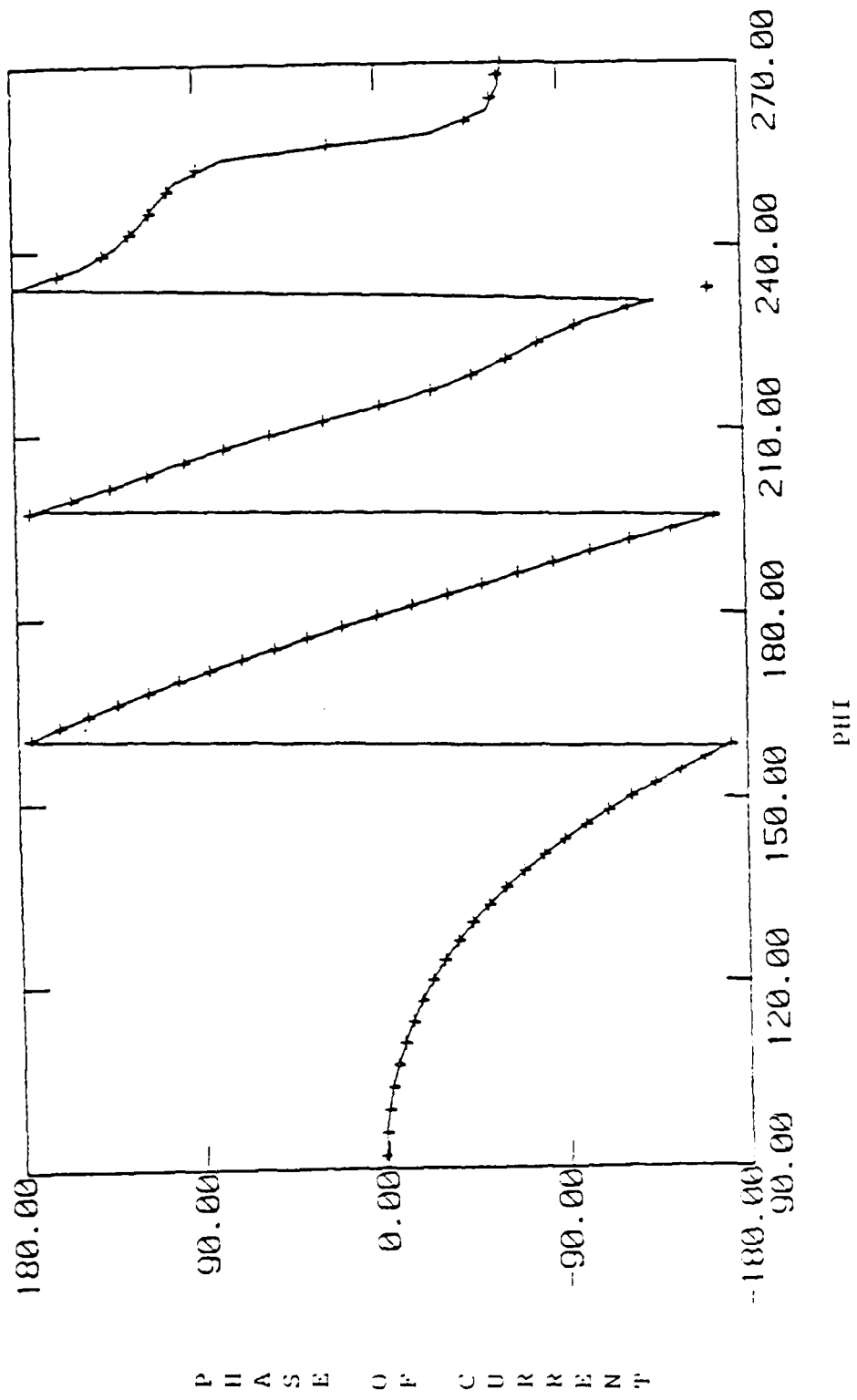
Figure 30. Phase of zero-order optics current on an elliptic cylinder of $a = 1.5\lambda$ with $\phi_i = 90^0$.

——— Exact Solution

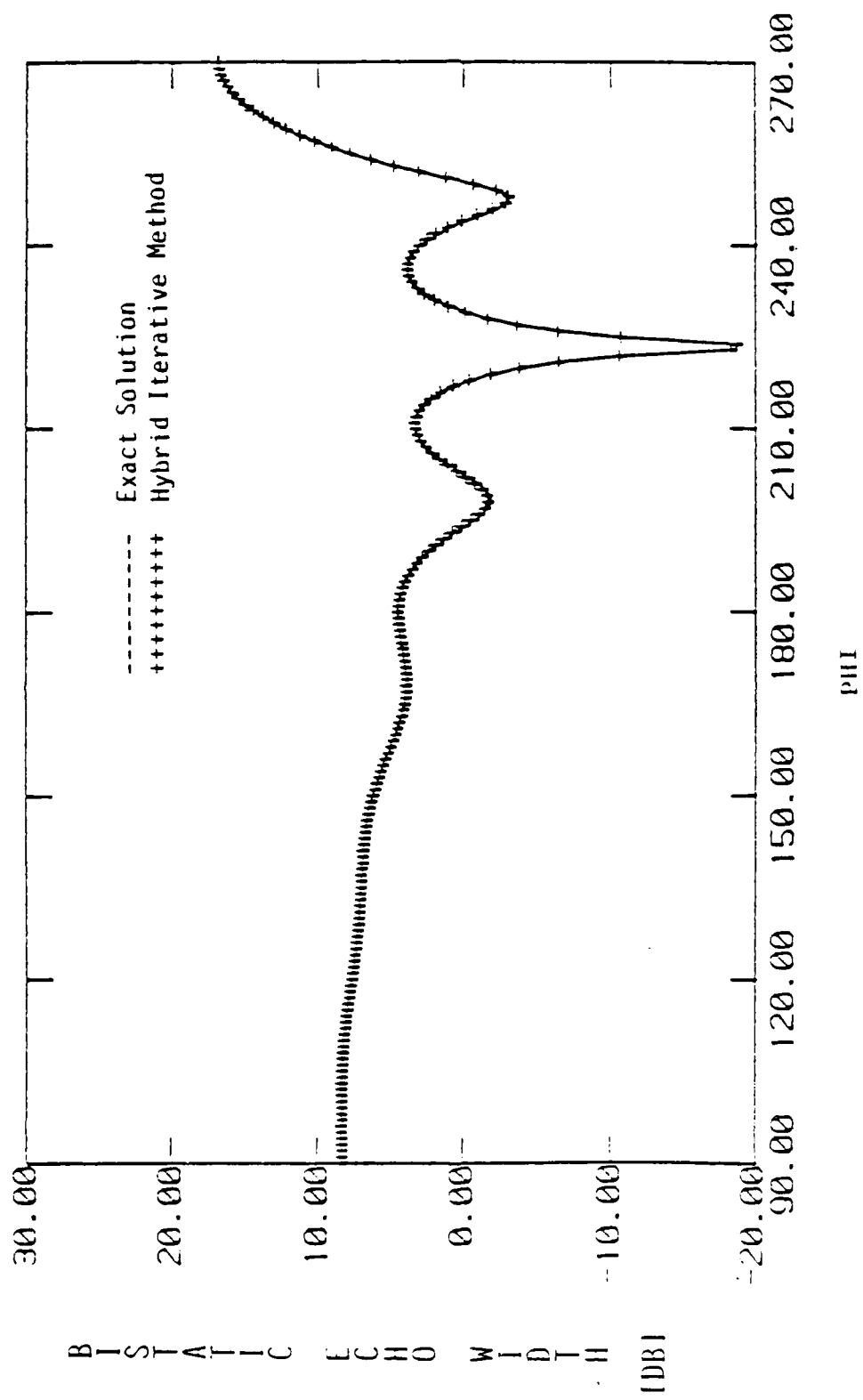++++++++++ Hybrid Iterative Method

Figure 31. Bistatic scattering pattern for an elliptic cylinder of $a = 1.5\lambda$ and $b = 1.0\lambda$ with $\phi_i = 90^0$.

VI. CONCLUDING REMARKS

In this report, we present a new technique, the hybrid-iterative technique, to compute the induced currents on an arbitrary, perfectly-conducting scatterer. This technique is obtained by incorporating the edge diffraction theory and Fock theory into the ansatz of the iterative technique for solving the magnetic field integral equation developed earlier [2]. Furthermore, the iterative scheme has been modified by computing higher-order "optics currents" instead of correction currents. We list the following advantages.

i)   Incorporating the edge diffraction theory and Fock theory eliminates the need for computing higher-order correction currents. That is, speed of convergence is improved. Frequently, zeroth order optics currents themselves furnish sufficiently accurate solutions. CPU time requirements are, therefore, less demanding.

ii) In the iterative technqiue, the shadow-side current is initially taken to be zero. This is inappropriate in some situations. This restriction is removed in this hybrid method. Hence, a wider class of problems may now be solved.

iii) Modifications in the iterative scheme introduced by replacing the evaluation of the correction currents by the evaluation of higher-order optics currents simplifies the computer code. As a result, savings in CPU time are effected.

It had already been established that our technique does not give spurious currents for frequencies corresponding to interior resonances of a scatterer. Furthermore, as the size of the body is increased our technique is

51

computationally more efficient than method of moments. As an example, our technique requires only one-third to one-quarter the CPU time required by the MM to compute the currents on a 3.7λ square cylinder. For larger scatterers, the advantage in CPU time is increasingly higher.

Even though the technique has been demonstrated only for 2-D, perfectly-conducting scatterers, it may be extended to more complicated structures like coated scatterers and 3-D bodies.

REFERENCES

1. T. J. Kim and G. A. Thiele, "A hybrid diffraction technique - general theory and applications," IEEE Trans. Antennas and Propagat., Vol. AP-30, pp. 888-897, 1982.

2. M. Kaye, P. K. Murthy and G. A. Thiele, "An iterative method for solving scattering problems," Accepted for publication in IEEE Trans. Antennas and Propagat..

3. M. Kaye, P. K. Murthy and G. A. Thiele, "An iteration method for complex scattering problems," RADC-TR-84-204, October 1984, Rome Air Development Center, New York.

4. G. T. Ruck, D. E. Barrick, W. D. Stuart and C. K. Krichbaum, "Radar cross-section handbook - Vol. 1," Plenum Press, New York (1970), pp.

5. P. K. Murthy and G. A. Thiele, "Closed form expressions for non-uniform currents on a wedge illuminated by a TE-plane wave". (In Preparation)

6. G. L. James, " Geometrical theory of diffraction for electromagnetic waves," Peter Perengrinus, Stevenage, England (1976), pp. 20-21.

7. R. F. Goodrich, "Fock Theory - An Appraisal and Exposition," IEEE Trans. Antennas and Propagat. Vol. AP-7, pp.528-536, December 1959.

8. S. C. Lee, "Control of electromagnetic scattering by antenna impedance loading," ElectroScience Lab., Dep. Elec. Eng., Ohio State Univ., Columbus, Rep. 3424-2, July 1974, prepared under contract F19628-72-C-0202 for A. F. Cambridge Res. Labs (AFLRL-TR-74-0426), also AP/A-004134.

9. W. Pogorzelski, "Integral Equations and Their Applications, Vol. 1," New York: Pergamon Press, 1966.

MISSION
of
Rome Air Development Center

RADC plans and executes research, development, test and selected acquisition programs in support of Command, Control, Communications and Intelligence (C³I) activities. Technical and engineering support within areas of competence is provided to ESD Program Offices (POs) and other ESD elements to perform effective acquisition of C³I systems. The areas of technical competence include communications, command and control, battle management, information processing, surveillance sensors, intelligence data collection and handling, solid state sciences, electromagnetics, and propagation, and electronic, maintainability, and compatibility.

DTIC

FILMED

4-86

END